DEVELOPMENT OF A CALCULATION METHODOLOGY TO DETERMINE DETECTOR RESPONSE IN A SPENT FUEL POOL

By

WILLIAM WALTERS

A THESIS PRESENTED TO THE GRADUATE SCHOOL
OF THE UNIVERSITY OF FLORIDA IN PARTIAL FULFILLMENT
OF THE REQUIREMENTS FOR THE DEGREE OF
MASTER OF SCIENCE

UNIVERSITY OF FLORIDA

2009

ACKNOWLEDGMENTS

I would like to thank my advisor, Dr. Alireza Haghighat, for his support and mentoring throughout this project. I would also like to thank Dr. Glenn Sjoden for his help and for his time to be on my thesis committee. Also, fellow graduate student Michael Wenner has proved indispensable for his work and insight on the project.

Finally, I would like to thank the sponsors of the project at LLNL, Dr. Shiva Sitaraman and Dr. Young Ham for their information and help on this work.

TABLE OF CONTENTS

page

LIST OF TABLES

LIST OF FIGURES

Abstract of Thesis Presented to the Graduate School
of the University of Florida in Partial Fulfillment of the
Requirements for the Degree of Master of Science

DEVELOPMENT OF A CALCULATION METHODOLOGY TO DETERMINE DETECTOR RESPONSE IN A SPENT FUEL POOL

By

William Walters

December 2009

Chair: Alireza Haghighat
Major: Nuclear Engineering Sciences

In this thesis we present a methodology for predicting the response of neutron and gamma detectors in a spent fuel pool (e.g., the Atucha-I reactor) with the aim of detecting gross misinformation (i.e., a missing or stolen fuel assembly). We expand on previous work by Ham et al.

To begin, the intrinsic decay sources of the spent fuel is calculated as a function of burnup and time. The burnup distribution in the fuel assembly under reactor conditions was calculated using a combination of ORIGEN-ARP depletion code and the MCNP Monte Carlo code. This calculation shows the non-linearity of the neutron source as a function of burnup and also takes into account the decay time, both of which were ignored previously. The sub-critical multiplication is calculated in the spent fuel pool by using a simplified fission matrix approach. The multiplication factor was found to be as high as ~2 and showed significant spatial variation.

The detector response was calculated using the detector importance methodology. The adjoint transport equation was solved using the PENTRAN Sn transport code. This importance calculation showed that ~87% of the neutron response comes from the surrounding 4 assemblies (i.e. one assembly in each direction) and 99% comes from

the nearest 16 (i.e. a distance of 2 assemblies in each direction). This contrasts the previous assumption that 100% of the response came from the 4 adjacent assemblies. This detector Field-Of-View (FOV) was relatively insensitive to detector position, showing ~5% difference for a detector at the edge of the pool vs. the middle of the pool. Assembly burnup was also not a large factor, showing less than ~5% difference between a fresh assembly and one at full burnup.

These results were combined to look at the predicted detector response for several hypothetical pool configurations. These configurations included the replacement of an assembly with either an inert dummy or a fresh assembly, replacement of several assemblies in a checkerboard pattern and attempted masking of a dummy assembly with a high burnup one. In all of these configurations the changes would be visible for a detector placed adjacent to the assemblies of interest, or on one of the corner assemblies for the checkerboard arrangement. A ratio of neutron response to gamma response was also investigated, but seemed less sensitive to different configurations than that of neutron signal only.

CHAPTER 1
INTRODUCTION

Methods for spent fuel pool verification can be difficult, especially if the spent fuel is tightly packed, e.g., the Atucha-I reactor in Argentina, due to interaction of detectors with many nearby assemblies. Spent fuel verification is extremely important with regards to non-proliferation, i.e. making sure that nuclear materials are not being diverted for illicit use. Previous work by Ham et al.[1] used a neutron detector placed in the assembly lattice, and assumed that the count rate would be proportional to the sum of the burnups of the four surrounding assemblies. While this approach is effective for low burnup fuel (5-8 GWd/t), it is not valid for higher burnups. This study seeks to create a more general methodology that is valid for all burnup levels and cooling times found in the spent fuel pool at Atucha-I as well as being able to include gamma detectors. In order to accomplish this, several improvements are made. First, the neutron and gamma sources in the assemblies are calculated explicitly as a function of total burnup and decay time. This avoids the assumption of response being linearly proportional to burnup. The detector field-of-view (FOV) (i.e. how many assemblies the detector "sees") is calculated using the importance function methodology[2,3]. This methodology provides detailed information on the regional and spectral contributions to the detector response. Finally, the neutron source distribution is modified by calculating the sub-critical multiplication in the spent fuel pool for more accurate predictions[4]. These methods are applied and analyzed for several hypothetical spent fuel configurations.

CHAPTER 2
THEORY

2.1 Radiation Transport Methods

In order to be able to determine the response of a detector to radiation fields, it is necessary to be able to calculate the neutron and gamma flux due to radiation sources. To solve this, we can either solve the Linear Boltzmann Equation directly or use the Monte Carlo method.

2.1.1 Linear Boltzmann Equation

The steady state Linear Boltzmann Equation (LBE) for a non-multiplying medium is described in Equation 2-1.

$$\hat{\Omega}\cdot\nabla\Psi(\underline{r},E,\hat{\Omega})+\sigma_t(\underline{r},E)\Psi(\underline{r},E,\hat{\Omega})= \int_0^\infty dE'\int_{4\pi} d\Omega'\sigma_s(\underline{r},E'\to E,\hat{\Omega}'\cdot\hat{\Omega})\Psi(\underline{r},E',\hat{\Omega}')+S(\underline{r},E,\hat{\Omega}) \quad (2\text{-}1)$$

Where, $\underline{r}$ is the spatial position vector (x,y,z) and $\hat{\Omega}$ is the unit vector in the direction of travel and is defined as shown by Equation 2-2

$$\hat{\Omega}=<\mu,\eta,\xi>=<\cos\theta,\sin\theta\cos\varphi,\sin\theta\sin\varphi> \quad (2\text{-}2)$$

Where, θ and ϕ are the standard polar and azimuthal angles, respectively.

The LBE represents a balance equation in a phase space. The first term is the particle streaming term. The second term represents collisions that remove the particle from the phase space (either complete absorption or scattering to a different energy or angle). The third term represents particles from every other energy and angle within $dE'd\hat{\Omega}'$ scattering into the current phase space within $dEd\hat{\Omega}$ of ($\underline{r}$,E, $\hat{\Omega}$). The fourth term represents an independent source (e.g. spontaneous fission neutrons).

2.1.2 Detector Importance Methodology

In a standard "forward" transport calculation, the linear Boltzmann transport equation (Equation 2-3) is solved in volume V in order to determine the angular flux Ψ.

$$H\Psi = S \tag{2-3}$$

Where, H is the transport operator given by Equation 2-4.

$$H = \hat{\Omega}\cdot\nabla + \sigma_t(\underline{r}, E) - \int_0^\infty dE' \int_{4\pi} d\Omega' \sigma_s(\underline{r}, E' \rightarrow E, \hat{\Omega}'\cdot\hat{\Omega}) \tag{2-4}$$

To determine the response of a detector for a given source and boundary condition, the angular flux is solved by Equation 2-3, and used in Equation 2-5.

$$R = < \Psi \sigma_d > \tag{2-5}$$

Where, < > denotes integration over all independent variables (space, energy and angle), and σ_d is the detector cross section.

In the adjoint or importance function methodology, the adjoint transport equation (Equation 2-6) is solved to determine the importance function Ψ^* due to an adjoint source S^* (or objective function)[2].

$$H^*\Psi^* = S^* \tag{2-6}$$

Where, the adjoint or importance transport operator is given by Equation 2-7.

$$H^* = -\hat{\Omega}\cdot\nabla + \sigma_t(\underline{r}, E) - \int_0^\infty dE' \int_{4\pi} d\Omega' \sigma_s(\underline{r}, E \rightarrow E', \hat{\Omega}'\cdot\hat{\Omega}) \tag{2-7}$$

If we define $S^* = \sigma_d$ and consider a vacuum boundary condition, i.e.,

$\Psi = 0$ on area Γ for $\hat{n}\cdot\hat{\Omega} < 0$, and

$\Psi^* = 0$ on area Γ for $\hat{n}\cdot\hat{\Omega} > 0$

Then, using a commutation formulation between the forward and adjoint equations (i.e., Equations 2-3 and 2-6), we obtain a new formulation for the detector response in terms of the importance function as in Equation 2-8.

$$R = < \Psi^* S > \tag{2-8}$$

Where, S is the standard "forward" source.

The importance function methodology allows for fast calculations of response given a variety of possible sources. This is very important for fuel verification since the source is not known completely. Using the importance function, we can determine the proportion of the detector response that comes from each assembly (i.e. the FOV). The fraction of the response due to one particular assembly is given by Equation 2-9.

$$FR_i = \frac{\sum_g \Psi_{ig}^* S_{ig}}{\sum_i \sum_g \Psi_{ig}^* S_{ig}} \tag{2-9}$$

Where, S_{ig} is the source located in assembly *i* in energy group *g*.

In this study, we use the importance methodology to predict detector responses in a spent fuel pool. To accomplish this, we need to do three things:

- Perform a fuel burnup calculation to determine the spent fuel composition
- Calculate the sub-critical neutron multiplication in the pool
- Solve the adjoint LBE to determine the detector importance function

2.1.3 Numerical Solution of the LBE

In order to solve the LBE (either in the forward or adjoint form) numerically, it must first be discretized in energy, angle and space.

2.1.3.1 Energy discretization

First, the LBE is integrated over G energy groups, resulting in the multi-group form of the LBE as given by Equation 2-10.

$$\hat{\Omega}\cdot\nabla\Psi_g(\underline{r},\hat{\Omega})+\sigma_{t,g}(\underline{r})\Psi_g(\underline{r},\hat{\Omega})=\sum_{g'=1}^{G}\int_{4\pi}d\Omega'\sigma_{s,g\to g'}(\underline{r},\hat{\Omega}'\cdot\hat{\Omega})\Psi_{g'}(\underline{r},\hat{\Omega}')+S_g(\underline{r},\hat{\Omega}) \qquad (2\text{-}10)$$

Where, we define the group flux and source in Equations 2-11 2-12.

$$\Psi_g(r,\hat{\Omega})=\int_{E_g}^{E_{g-1}}dE\Psi(\underline{r},E,\hat{\Omega}) \text{ for } g=1,G \qquad (2\text{-}11)$$

$$S_g(r,\hat{\Omega})=\int_{E_g}^{E_{g-1}}dES(\underline{r},E,\hat{\Omega}) \text{ for } g=1,G \qquad (2\text{-}12)$$

Where, E_g represents the upper energy boundary for group g. This also requires that a group cross section be defined, e.g., Equation 2-13.

$$\sigma_g(r)=\frac{\int_{E_g}^{E_{g-1}}\sigma(r,E)\phi(r,E)dE}{\int_{E_g}^{E_{g-1}}\phi(r,E)dE} \qquad (2\text{-}13)$$

The group scattering cross-section $\sigma_{s,g\to g'}$ is defined in an analogous way.

Multi-group cross section generation is one of the main difficulties of the deterministic method, since it requires the flux spectrum to be known (or have a good guess) beforehand. This source of error can be mitigated by using an appropriate energy group structure and spectrum.

2.1.3.2 Angular quadrature and scattering expansion

For the angular variable, we consider that the equations hold over a number of distinct angles Ω_n. From here, we translate the integrals over $\hat{\Omega}$ into sums over $\hat{\Omega}_n$ as in Equation 2-14.

$$\int_{4\pi} d\Omega f(\hat{\Omega}) = \sum_n w_n f(\hat{\Omega}_n) \tag{2-14}$$

The quadrature set of weights w_n and angles Ω_n are chosen such that the angular flux is well represented and various properties are preserved. A standard set is the so called Nth order level-symmetric quadrature, which results in N(N+2) distinct directions.

The scattering cross section is dealt with by expanding it in a series of Legendre polynomials as in Equation 2-15. This series is truncated at order L. This is called the P_L expansion to the scattering cross section.

$$\sigma_{s,g'\to g}(r,\hat{\Omega}'\cdot\hat{\Omega}) = \sum_{l=0}^{L}(2l+1)\sigma_{s,g'\to g,l}(r,\hat{\Omega}'\cdot\hat{\Omega})P_l(\hat{\Omega}'\cdot\hat{\Omega}) \tag{2-15}$$

Using these, we can now write the Legendre expanded discrete ordinates multi-group form of the LBE in Cartesian geometry (Equation 2-16)[5].

$$\begin{aligned}&\left(\mu_n\frac{\partial}{\partial x}+\eta_n\frac{\partial}{\partial y}+\xi_n\frac{\partial}{\partial z}\right)\psi_g(x,y,z,\mu_n,\varphi_n)+\sigma_{t,g}(x,y,z)\psi_g(x,y,z,\mu_n,\varphi_n)=\\&\sum_{g'=1}^{G}\sum_{l=1}^{L}(2l+1)\sigma_{s,g'\to g,l}(x,y,z)\{P_l(\mu_n)\phi_{g,l}(x,y,z)+2\sum_{k=1}^{l}\frac{(l-k)!}{(l+k)!}P_l^k(\mu)\cdot\\&[\phi^k_{C\,g',l}(x,y,z)\cos(k\varphi_n)+\phi^k_{S\,g',l}(x,y,z)\sin(k\varphi_n)]\}+S_g(x,y,z,\mu_n,\varphi_n)\end{aligned} \tag{2-16}$$

μ_n = x direction cosine for angular ordinate n
η_n = y direction cosine for angular ordinate n
ξ_n = z direction cosine for angular ordinate n
ψ_g = group g angular particle flux (for groups g=1,G)
φ_n = azimuthal angle constructed from arctan(ξ/η), with proper phase shift
$\sigma_{t,g}$ = total group macroscopic cross section

l = Legendre expansion (*l=0,L), L*=0 or odd truncation

$\sigma_{s,g'\to g,l}$ = l^{th} Legendre moment of the macroscopic differential scattering cross section from group g' to g

$P_l(\mu)$ = l^{th} Legendre polynomial

$\phi_{g,l}$ = l^{th} Legendre scalar flux moment for group g

$P_l^k(\mu)$ = l^{th}, k^{th} Associated Legendre polynomial

$\phi^k_{C\,g',l}$ = l^{th}, k^{th} Cosine Associated Legendre scalar flux moment for group g

$\phi^k_{S\,g',l}$ = l^{th}, k^{th} Sine Associated Legendre scalar flux moment for group g

The flux moments $\phi_{g,l}$, $\phi^k_{C\,g',l}$, $\phi^k_{S\,g',l}$ are defined in terms of the angular flux ψ_g by Equations 2-17, 2-18 and 2-19.

$$\phi_{g',l}(x,y,z)=\int_{-1}^{1}\frac{d\mu'}{2}P_l(\mu')\int_0^{2\pi}\frac{d\varphi'}{2\pi}\psi_{g'}(x,y,z,\mu',\varphi') \tag{2-17}$$

$$\phi^k_{C\,g',l}(x,y,z)=\int_{-1}^{1}\frac{d\mu'}{2}P_l^k(\mu')\int_0^{2\pi}\frac{d\varphi'}{2\pi}\cos(k\varphi')\psi_{g'}(x,y,z,\mu',\varphi') \tag{2-18}$$

$$\phi^k_{S\,g',l}(x,y,z)=\int_{-1}^{1}\frac{d\mu'}{2}P_l^k(\mu')\int_0^{2\pi}\frac{d\varphi'}{2\pi}\sin(k\varphi')\psi_{g'}(x,y,z,\mu',\varphi') \tag{2-19}$$

2.1.3.3 Spatial differencing

For the space variable, we integrate the LBE over spatial cells, which eliminates the derivative term as in Equation 2-20.

$$\begin{aligned}\frac{1}{\Delta x\Delta y\Delta z}\int_{z_{k-1/2}}^{z_{k+1/2}}dz\int_{y_{j-1/2}}^{y_{j+1/2}}dy\int_{x_{i-1/2}}^{x_{i+1/2}}dx\hat{\Omega}\cdot\nabla\Psi_{n,g}(x,y,z)&=\frac{\mu_n}{\Delta x_i}(\Psi_{n,i+1/2,j,k,g}-\Psi_{n,i-1/2,j,k,g})\\&+\frac{\eta_n}{\Delta y_j}(\Psi_{n,i,j+1/2,k,g}-\Psi_{n,i,j-1/2,k,g})+\frac{\xi_n}{\Delta z_k}(\Psi_{n,i,j,k+1/2,g}-\Psi_{n,i,j,k-1/2,g})\end{aligned} \tag{2-20}$$

Where, $x_{i-1/2}$, $x_{i+1/2}$, $y_{j-1/2}$, $y_{j-1/2}$, $z_{k-1/2}$, $z_{k+1/2}$ represent the (x,y,z) boundaries of spatial cell (i,j,k). $\Psi_{n,i+1/2,j,k}$, $\Psi_{n,i-1/2,j,k}$, $\Psi_{n,i,j+1/2,k}$, $\Psi_{n,i,j-1/2,k}$, $\Psi_{n,i,j,k+1/2}$, and $\Psi_{n,i,j,k-1/2}$ represent

the angular fluxes on the boundary of cell (*i,j,k)*. The average angular flux in each cell is defined by Equation 2-21.

$$\Psi_{n,i,j,k,g} = \frac{1}{\Delta x \Delta y \Delta z} \int_{z_{k-1/2}}^{z_{k+1/2}} dz \int_{y_{j-1/2}}^{y_{j+1/2}} dy \int_{x_{i-1/2}}^{x_{i+1/2}} dx \Psi_{n,g}(x,y,z) \tag{2-21}$$

The cell average source $S_{i,j,k,g}$ is calculated in the same fashion.

Of the 6 surface fluxes in cell (*i,j,k*) (e.g. $\Psi_{n,i+1/2,j,k,g}$), 3 are known due to the known boundary conditions, but this leaves three unknowns. This is solved by using a spatial differencing scheme, such as the Diamond Differencing scheme, expressed by Equation 2-22.

$$\begin{aligned} \Psi_{n,i,j,k,g} &= \frac{1}{2}\Psi_{n,i+1/2,j,k,g} + \frac{1}{2}\Psi_{n,i-1/2,j,k,g} \\ &= \frac{1}{2}\Psi_{n,i,j+1/2,k,g} + \frac{1}{2}\Psi_{n,i,j-1/2,k,g} \\ &= \frac{1}{2}\Psi_{n,i,j,k+1/2,g} + \frac{1}{2}\Psi_{n,i,j,k-1/2,g} \end{aligned} \tag{2-22}$$

Using the three additional equations, we can solve for the three unknowns. This simplistic approximation is accurate if the flux is not changing rapidly across the cell. However, for large, optically thick cells this can yield large errors, and more sophisticated methods are generally used.

2.1.3.4 PENTRAN

The PENTRAN code[5] is used here to iteratively solve the multigroup LBE in 3-D Cartesian coordinates using S_N angular quadrature and P_L Legendre polynomial expansion for the scattering term. PENTRAN includes an adaptive differencing strategy which automatically and intelligently changes the spatial differencing scheme based on the problem physics. Parallel decomposition in space, angle and/or energy allows for

large problems to be distributed over many computers. Acceleration schemes, such as coarse mesh rebalance and multigrid methods are available to improve convergence rate.

2.1.2 Monte Carlo Method

The Monte Carlo method is a way to solve the radiation transport problem in a statistical fashion. Instead of trying to solve the LBE directly, we simulate the stochastic processes of many individual particles in an attempt to determine the average or expected particle behavior[2].

2.1.2.1 Random variables

A random process can be described by its probability density function (pdf, $p(x)$) and its cumulative density function (cdf, $P(x)$).

$p(x)dx$ represents the probability of a sample being drawn between x and $x+dx$. $P(x)$ represents the probability of a sample being drawn that is *less than* x. The two are related by Equation 2-23.

$$P(x) = \int_{-\infty}^{x} p(x')dx \tag{2-23}$$

Commonly, a pdf is normalized as in Equation 2-24.

$$\int_{-\infty}^{\infty} p(x)dx = 1 \tag{2-24}$$

Radiation interactions are an inherently stochastic process. It is impossible to tell in advance how far a neutron of a given energy will travel in a given material before interacting. However, we do know the probability densities associated with various fundamental interactions/processes (e.g., scattering, fission, absorption).

2.1.2.2 Random variable sampling

In general, we know the probabilities for all the interactions that occur to a particle. To simulate individual particles, we must sample from these distributions. To do this we first generate a random number η whose probability function is described by Equation 2-25.

$$p(\eta) = 1 \ for \ 0 < \eta < 1 \tag{2-25}$$

These random numbers η are typically generated using a pseudo-random number generator (PRNG) on a computer. The random numbers can then be used to sample from a probability distribution p(x) using Equation 2-26, known as the Fundamental Formulation of Monte Carlo (FFMC). This equation always has exactly one solution, as η is between 0 and 1, and $P(x)$ is a monotonically increasing function between 0 and 1.

$$\eta = P(x) = \int_{-\infty}^{x} p(x')dx' \tag{2-26}$$

In the case of the distance traveled by a particle before an interaction the sampled distance x_i can be calculated in terms of the random number η_i in Equation 2-27.

$$x_i = \frac{-\ln(\eta_i)}{\sigma} \tag{2-27}$$

In this fashion, we can simulate many particles from their "birth" as a source particle, through scattering, free flight, etc., until their "death" by absorption or leakage from the system.

2.1.2.3 Criticality calculation

In a fixed source calculation, the starting location of a source particle is simply sampled from the source distribution $S(x,y,z)$. For a criticality calculation, this source is not known to begin with, and is in fact one of the goals of the simulation. To start the

simulation, N neutrons are started at some points withinin the fuel regions. These neutrons travel around, and some of them cause fission. When the fission occurs, the new born neutrons are stored in a bank for the next generation. After all the particles of the generation have finished, the next generation is started, using the bank of fission neutrons created in the previous generation. This process is continued for many cycles, until eventually this source distribution is settled to the "true" distribution. After this time, the multiplication factor (k) of each generation n is evaluated by Equation 2-28.

$$k_n = \frac{N_n}{N_{n-1}} \tag{2-28}$$

Where, N_n represents the number of source neutrons in generation n. These generations are continued until an average multiplication factor (k) with sufficient precision is obtained.

2.1.2.4 Tallying and uncertainty

In order to calculate the expected value of some desired quantity (say, the probability of transmission through a shield), we use particle tallies. In this case we count the proportion of particles that transmit through the shield vs. the total number of source particles.

Since we are performing many random samples, we expect to calculate a mean $\bar{x}$ that will have an associated variance σ^2. According to the Central Limit Theorem, for a large number of samples, we expect that our calculated value $\bar{x}$ will be normally distributed around the true value of our desired result m with a variance of σ^2. If the samples that make up $\bar{x}$ are independent, and the number of samples is large, the variance will be given by Equation 2-29.

$$R_{\bar{x}} = \frac{\sigma}{\bar{x}} = \sqrt{\frac{\sum_{i=1}^{N} x_i^2}{\left(\sum_{i=1}^{N} x_i\right)^2} - \frac{1}{N}} \tag{2-29}$$

As a result of the random nature of the Monte Carlo process, we can never expect to get the exact answer. The result $\bar{x}$ will always have some statistical uncertainty associated with it.

2.1.2.6 Benefits and drawbacks of Monte Carlo

The main advantage of Monte Carlo is the lack of discretization that is required for a deterministic calculation. The multi-group cross sections, spatial grids and angles can incur significant inaccuracies in the deterministic method, unlike Monte Carlo, which uses continuous energy, space and angle. Due to the excellent accuracy, Monte Carlo is often used to benchmark the accuracy of deterministic algorithms.

The biggest drawback of Monte Carlo is the computation time. In order to get statistical uncertainties that are acceptable, Monte Carlo can take a prohibitive amount of time. Another advantage that the deterministic method has is the quantity of information. The calculation will provide the angular flux for all space, energies and angles. In Monte Carlo, usually only specific tallies are recorded. More information is possible by using many tallies, but the computation time very quickly increases in order to get answers within the required uncertainty.

2.1.2.6 MCNP

The MCNP (Monte Carlo N-Particle) code[6] is used in this thesis to perform the Monte Carlo calculations. MCNP is a general purpose Monte Carlo neutron, photon, and/or electron transport code developed at Los Alamos National Lab. It supports the

use of point-wise (or continuous energy) cross-sections as well as exact Boolean geometry using volumes bounded by up to 4th order surfaces. MCNP also has the ability to run in criticality or fixed source mode, both of which are required for the work in this thesis.

2.2 Assembly Burnup Calculation

In a reactor environment, the differential equation for the number N_i of every isotope i can be expressed by Equation 2-30.

$$\frac{dN_i}{dt} = \sum_j \lambda_{j\to i} N_j - \lambda_i N_i + \sum_k \overline{\gamma_{ki}\sigma_{f,k}} N_k \phi + \overline{\sigma}_{\gamma,i-1}\phi N_{i-1} - \overline{\sigma}_{a,i}\phi N_i \qquad (2\text{-}30)$$

In order, the terms on the right represent:

- (+) Decay rate of isotope j into isotope i (by β^+, β^-, or α decay)
- (-) Decay rate of isotope i
- (+) Fission yield rate from fission of isotope k to isotope i
- (+) Neutron absorption rate from isotope i-1 to i
- (-) Neutron absorption rate of isotope i

In this equation, λ_{ji} and λ_i are known material decay constants and γ_{ki} is the fission yield. The initial concentration of all isotopes $N_i(t=0)$ is known. The reactor flux ϕ is determined by the reactor power as given in Equation 2-31.

$$P = \sum_k \overline{G}_{f,k}\overline{\sigma}_{f,k} N_k \phi \qquad (2\text{-}31)$$

Where, P is the total reactor power and $G_{f,k}$ is the energy released per fission for isotope k. The averaged cross sections are calculated by Equation 2-32.

$$\overline{\sigma} = \frac{\int_0^\infty \phi(E)\sigma(E)dE}{\int_0^\infty \phi(E)dE} \tag{2-32}$$

ORIGEN-ARP code[7], a module in the SCALE 5.1 code package[8], is used to perform the burnup and decay calculation. The averaged cross sections are obtained by ORIGEN-ARP by interpolating a set of pre-computed burnup-dependent cross sections that are available for a number of different fuel types.

2.3 Sub-critical Multiplication

In a multiplicative system, the eigenvalue k represents the number of neutrons generated for each neutron born. In a reactor, k is exactly 1 and there is equilibrium. If *k* is less than one, the reaction will die out. However, if there is an external independent source of neutrons, the net result is a multiplication of the source strength. If S_0 neutrons start in generation 1, then in generation 2 there will be kS_0. In generation 3 there will be $k \cdot kS_0 = k^2 S_0$, and so on. If this series is continued, the total source due to the multiplication can be seen in Equation 2-33.

$$S_m = S_0(k + k^2 + k^3 + k^4 + ...) \tag{2-33}$$

If k<1, the above infinite series converges to Equation 2-34.

$$S_m = S_0 \frac{k}{1-k} \tag{2-34}$$

The source multiplication factor is defined by Equation 2-35.

$$M = \frac{S_m + S_0}{S_0} = S_0 \frac{1}{1-k} \tag{2-35}$$

CHAPTER 3
SPENT FUEL SOURCE CHARACTERIZATION

In order to predict the detector response using the importance function methodology, our first step is to determine the total neutron source distribution in the pool (i.e., S_{ig} in Equation 2-9). To calculate this term, we first simulate the burnup of the assembly under reactor conditions, which yields the material composition and thus the intrinsic source of neutrons and gamma rays due to decay, (α,n) reactions and spontaneous fission of certain isotopes. Next, we examine the process of neutron sub-critical multiplication in the spent fuel pool that creates an additional source of neutrons.

3.1 Assembly Intrinsic Source and Material Properties

To determine the intrinsic source and material properties of the spent fuel assemblies, we must simulate the burnup and decay processes. To do this, we first estimated the burnup distribution throughout each assembly using known reactor properties. With these estimated burnup values, a burn and decay calculation was performed resulting in the intrinsic source and material composition.

3.1.1 Assembly Burnup Distribution

Fuel assemblies at the Atucha-I reactor are circular with 36 fuel elements and one support rod. Figure 3-1 shows a schematic of an Atucha fuel assembly. The 5.3 m long assemblies are arranged in a hexagonal lattice of pitch 27.2 cm with heavy water acting as coolant and moderator. Fuel pellets are UO_2, either natural uranium (NU) or slightly enriched uranium (SEU, 0.85 w% enriched). Detailed Atucha-I properties are shown in Table 3-1[9,10,11].

In order to determine the burnup distribution of the fuel, an MCNP model was made with one fuel assembly in an infinite lattice, as shown in Figures 3-2 and 3-3.

Fresh SEU fuel was simulated, and the effects of control rods, burnable poisons or dissolved boron were not considered.

A criticality calculation was performed with MCNP, using 1000 skipped cycles, 2000 active cycles and 1000 histories per cycle. The MCNP input deck can be seen in Appendix A. The estimated eigenvalue is 1.18841 $\pm$ 0.00049. Neutron flux and fission rate were tallied throughout the assembly for each rod and in 10 axial locations. Figures 3-4 and 3-5 show the x-y flux distribution in the model for thermal (0-0.175 eV) and fast (1-20 MeV) energy groups, respectively. These plots show a depression of thermal flux in the center of the assembly, with the opposite effect for the fast flux. The fission distribution by fuel pin and axial position is shown in Figure 3-6. Fuel pins closest to the structural pin had the highest fission rate, due to a lack of absorption that would otherwise occur at the pin location. However, the largest spatial difference was the radial position, with the most fission occurring in the outer fuel pins.

To simplify the model, the difference in burnup of fuel pins at a given radial position was ignored and each assembly was homogenized into 3 radial rings as shown in Figure 3-7. In the axial direction, the first 3 axial zones were combined due to their similar fission rate, resulting in 8 axial levels. A simple volume-based homogenization was performed.

Another simplification was to assume that the spatial fission distribution did not change throughout the burnup cycle. This assumption means that the burnup at each location is proportional to the fission distribution in fresh fuel. Using the fission distribution and the total known burnup of the assembly, it was possible to assign a

specific local burnup value to each zone (3 radial zones and 8 axial levels). This is calculated by Equation 3-1.

$$B_i = \overline{B} V_T \frac{V_i \phi_i \sigma_{f,i}}{\sum_j V_j \phi_j \sigma_{f,j}} \quad (3\text{-}1)$$

Where, B_i is the local burnup in zone i, $\overline{B}$ is the average total assembly burnup, V_T is the total fuel volume in the assembly, V_i is the fuel volume in zone i, and $\phi_i \sigma_{f,i}$ is the fission density in zone i. Table 3-2 shows the relative local burnup (i.e., $B_i / \overline{B}$) for each axial and radial zone. The highest burnup is in axial zone one and the outer radial zone, with a burnup of 1.42 $\overline{B}$. The lowest burnup is in axial zone eight and the inner radial radial zone, with a burnup of 0.41 $\overline{B}$. The burnup increases with radial position and decreases by axial zone.

3.1.2 Burnup and Decay Calculation

For each of the burnup zones determined earlier, a burnup and decay calculation was performed using ORIGEN-ARP (Automatic Rapid Processing). ORIGEN-ARP has cross-section libraries of standard fuel assemblies across a range of burnups. The Atucha-I type fuel was not available, but the CANDU 37-element design was; this is very similar to Atucha-I. These calculations produced a database of material compositions and source strength as a function of location within the assembly, total burnup and decay time. Figure 3-8 shows the total neutron source strength as a function of local burnup and decay time. Figure 3-9 shows the gamma source. Both figures are for natural uranium fuel. Figures 3-10 and 3-11 show the same sources but as a function of decay time. Table 3-3 shows neutron source contribution by source and reaction type.

Figures 3-9 and 3-11 indicate that the gamma source is approximately linear with burnup and decays relatively quickly (from 1.7E16 to 7.0E14 photons/MTU/s for 1 and 30 years, respectively for a local burnup of 7000 MWd/MTU). Figures 3-8 and 3-10 show that the neutron source is non-linear (slope increasing with burnup) and decays slower than the gamma source (from 4.9E6 to 2.2E6 neutrons/MTU/s for 1 and 30 years, respectively for a local burnup of 7000 MWd/MTU). In terms of relative magnitude, the gamma source is much larger, by a factor of approximately 10^9.

The source terms calculated above were then used to create a source database. Given an assembly of arbitrary burnup and decay time, the source database can be interpolated to determine the source strength in each assembly zone.

3.2 Subcritical Multiplication

In order to use the adjoint methodology (Equation 2-8) it is necessary to have the total source (Equation 3-2) including any sub-critical multiplication, not just the intrinsic source.

$$S_{total} = S_{intrinsic} + S_{multiplication} \tag{3-2}$$

The spent fuel assemblies still contain significant amounts of fissile U-235, Pu-239 and Pu-241. The amount of fissile materials is too low for the pool to go critical (i.e. k=1), but there is enough to allow significant sub-critical (k<1) neutron multiplication. In a steady-state system with intrinsic source S_0 and sub-critical eigenvalue k<1, the total source S is given by Equation 3-3.

$$S = S_0 \frac{1}{1-k} = S_0 M \tag{3-3}$$

The sub-critical multiplication results in the need to calculate the multiplication source for each assembly in the pool. This could be done by a brute force fixed source

calculation, but this would be very time consuming and would have to be redone for any changes in the pool (e.g. addition of new assemblies).

For this work, it was decided to use a simplified fission matrix method. This involves using several full transport calculations at the beginning to characterize the properties of the pool, but results in a simple set of linear equations that can be solved quickly for any subsequent assembly arrangement.

3.2.1 Fission-Matrix Method

The fission matrix method describes the fission source strength in a spatial cell i due to itself and all other cells within a model. Equation 3-4 expresses the fission matrix formulation.

$$F_i = \sum_{j=1}^{N} a_{i,j}(F_j + S_j) \tag{3-4}$$

Where F_i is the induced fission source strength in cell i, S_i is the intrinsic source strength in cell i, $a_{i,j}$ is the number of neutrons directly produced in cell i due to a neutron born in cell j, and N is the total number of cells. In this study, each cell was considered to be an entire assembly for simplicity. Future work may require a finer cell structure, which can be easily accomplished using this method.

The fission matrix method results in a set of N linear equations, which can be easily solved for F given S and the $a_{i,j}$ coefficients. For this work, the Gauss-Seidel iterative method was used.

This approximation assumes that the spatial distribution (but not total strength) of F and S in each cell is the same. This is a good approximation for the interior of the pool, where the fission source should be reasonably flat, but can break down near the

edges where the fission source within an assembly will be skewed towards the center of the pool where the fission inducing neutrons are coming from.

3.2.2 Calculation of Fission-Matrix Coefficients

In the standard form, the fission matrix method is just as time-consuming as a full transport calculation because every coefficient must be calculated using transport. However, due to the repetitive nature of the spent fuel array, many of the coefficients are almost identical. If we assume that they are in fact identical, then the number of calculations required can be greatly reduced.

In order to simplify this calculation, it was assumed that the assemblies in the array could be divided into three categories: corner (i.e. 3 adjacent assemblies), edge (i.e. 5 adjacent assemblies) and interior (i.e. 8 adjacent assemblies). A model of the spent fuel pool showing these categories is shown in Figure 3-12. Schematics of the spent fuel pool are shown in Figures 3-13 and 3-14.

For each of the three assembly categories, a Monte Carlo calculation was performed using the MCNP (Monte Carlo N-Particle) code system. See Appendix B for the input deck used for the interior source calculation. The sample model was a 6x9 array of assemblies with 0.5m water shielding around the edges and a vacuum boundary on all sides. The source was located in a single assembly in the appropriate location (i.e. corner, edge or interior). The spatial distribution and energy spectrum of the source were taken from that of an average-burnup assembly. The number of direct fission neutrons produced in every assembly was tallied per source particle, giving the $a_{i,j}$ coefficients for three values of i. Coefficients less than 1E-4 were ignored, and the remaining coefficients were increased by a factor to conserve total reaction rate. This 1E-4 cutoff limited interactions to a distance of two assembly positions away in each

direction. Results for a NU assembly comparing the coefficients between the three different geometric cases are shown in Tables 3-4, 3-5 and 3-6. Figure 3-14 shows the convention for relative assembly position. The results show very little difference in relative fission matrix coefficients based on source position (<1% between interior and corner). However, this difference was slightly higher (2%) for SEU fuel in the more compact assembly arrangement. If slightly lower accuracy is acceptable then the additional Monte Carlo calculations could be avoided.

These calculated baseline $a_{i,j}$ coefficients were then used to create an entire $a_{i,j}$ matrix for an array of arbitrary size (provided the same geometric spacing between arrays). This is done by assuming that for a given location type (e.g. interior), the $a_{i,j}$ coefficients for an assembly relative to its surrounding assemblies are identical. For example, $a_{i,j}$ for every "interior" assembly to either neighbor in the x-direction are identical and equal to that calculated for the "interior" source above. Using this geometric similarity it is possible to estimate the entire fission matrix. If the spatial mesh is refined further, the same relative geometry considerations may be used to complete the matrix.

3.2.3 Fission-Matrix Method Verification

In order to check the results from the fission matrix method, four sample problems were devised, based on Atucha-I pool geometry, with various assembly array sizes and source distributions. For these problems, all assemblies were assumed to be identical NU assemblies with burnup of 5000 MWd/MTU and cooling time of 5 yrs. The problem descriptions are given below.

- 2x6 array, uniform source
- 9x6 array, uniform source

- 9x6 array, 27 assemblies on the left with source strength 1, the rest with source strength 0.5
- 20x6 array, uniform source

For each of these problems, an MCNP calculation was performed and the induced fission source was tallied in each assembly. As a metric of performance, the total multiplication factor (Equation 3-5) was calculated for the fission matrix method as well as the Monte Carlo method. Results for each sample case are shown in Table 3-7. See Appendix C for the script used to solve the fission matrix equations. The simplified fission matrix model does an excellent job of predicting the multiplication factor for a wide variety of situations. The same $a_{i,j}$ coefficients were used for every situation, so only three total MCNP calculations were performed for the fission matrix method.

$$M = \frac{\sum_{i=1}^{N} F_i + S_i}{\sum_{i=1}^{N} S_i} \tag{3-5}$$

As for the individual F_i components, none of these differed from MCNP by more than 5%. The average individual MCNP assembly tally error was 1%. A graph comparing the results of the F_i components for the 9x6 case with a non-uniform source is shown in Figure 3-17.

3.2.4 Compensation for Burnup and Cooling Time

In order to take into account different assembly burnups and decay times, the fission-matrix coefficients were calculated at several burnup values and decay times, and these coefficients were interpolated to each given assembly parameters. To test the accuracy of this method, a test problem was used in which the 9x6 array was filled with three 3x6 sections of different burnup and cooling time. The first section was 5000

MWd/MTU and 1yr cooling time. The middle section was 6500 MWd/MTU and 10 years cooling time. The Last section was 8000 MWd/MTU and 30 years cooling time. The fission-matrix coefficients for the first and third materials were calculated directly while the middle section was interpolated in burnup and cooling time. Results for the neutron multiplication calculations are shown in Figure 3-16.

3.2.5 Fission-matrix Calculation Time

The fission matrix method required three MCNP calculations in order to calculate the coefficients; each calculation takes approximately one hour. If there are large variations in assembly burnup and cooling time, then this process must be repeated three additional times at different burnups and cooling times in order to get values to interpolate the coefficients. Subsequent calculations using these coefficients took less than one second, as compared to one hour to achieve 1% uncertainty with the MCNP (in addition to calculating material properties for each assembly).

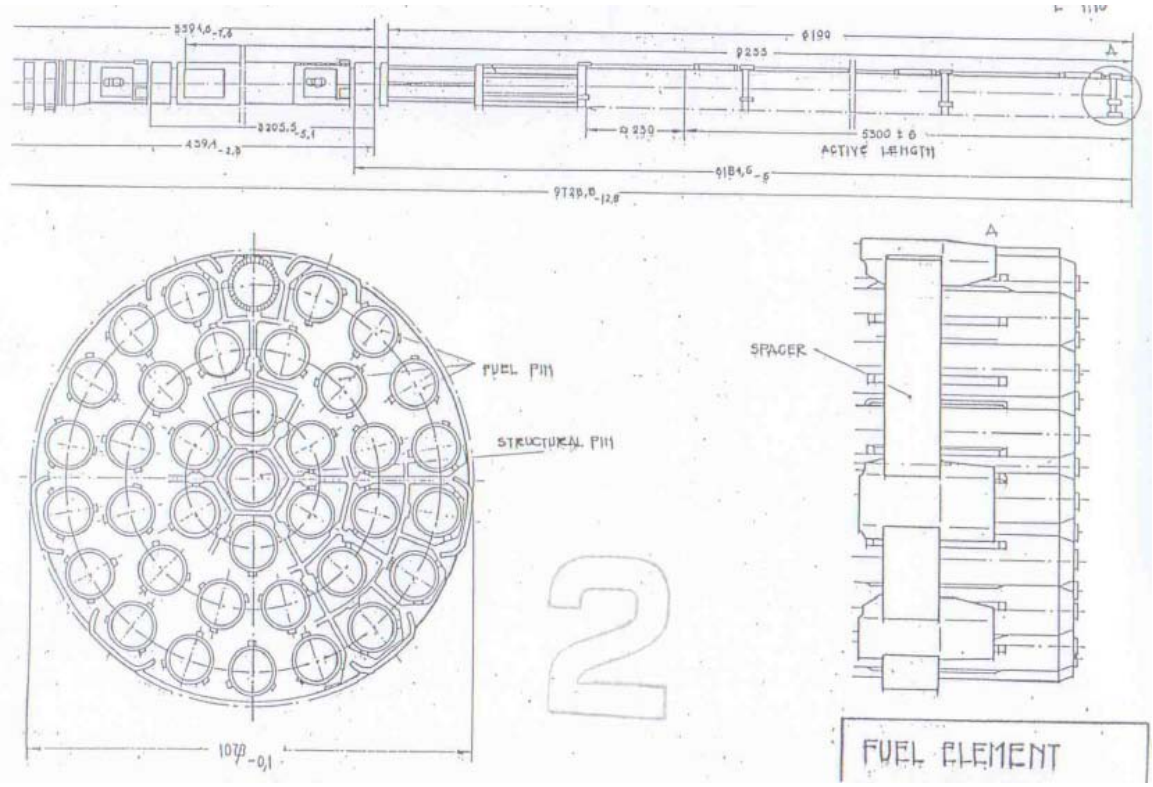

Figure 3-1. Schematic of an Atucha-I fuel assembly

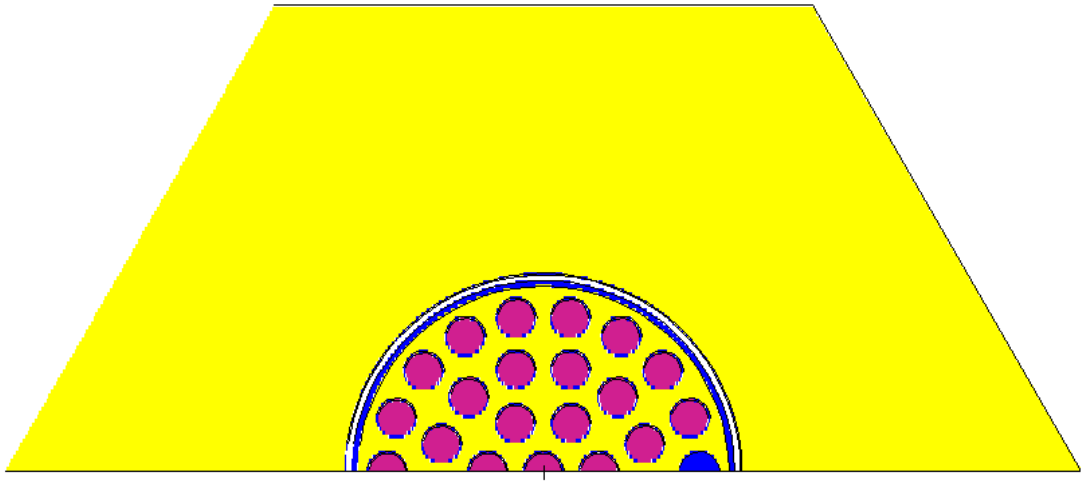

Figure 3-2. X-Y view of MCNP criticality model. Fuel is in purple, heavy water is yellow, and structural pin is in blue. Top/bottom/sides are all reflected.

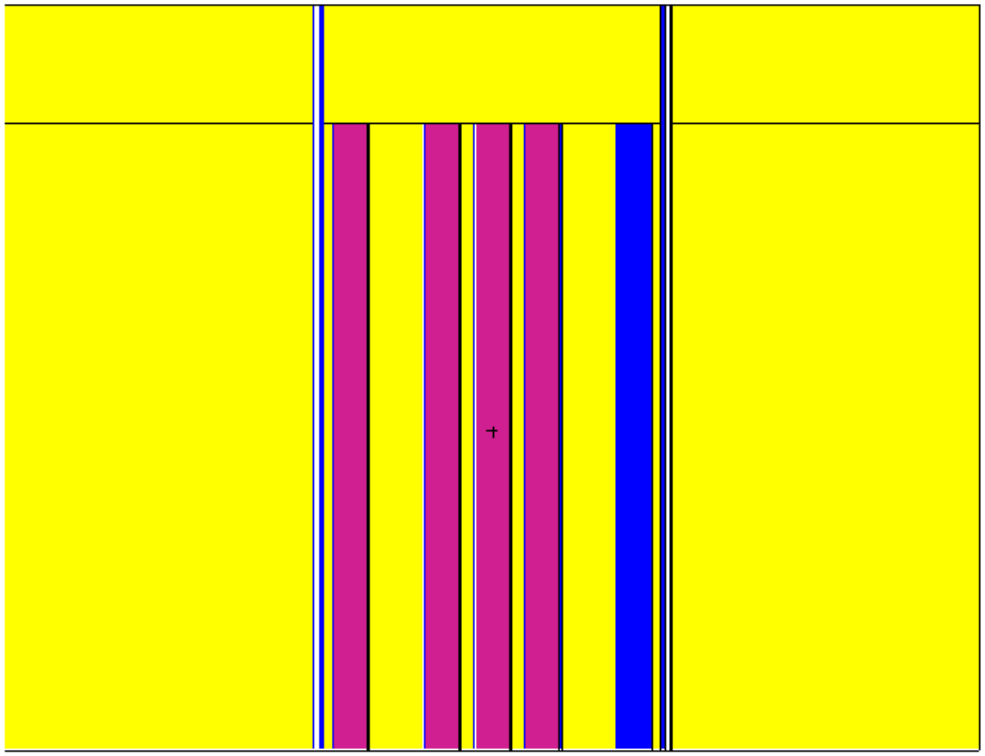

Figure 3-3. X-Z view of MCNP criticality model. Fuel is in purple, heavy water is yellow, and structural pin is in blue. Bottom/sides are all reflected. The top boundary is vacuum

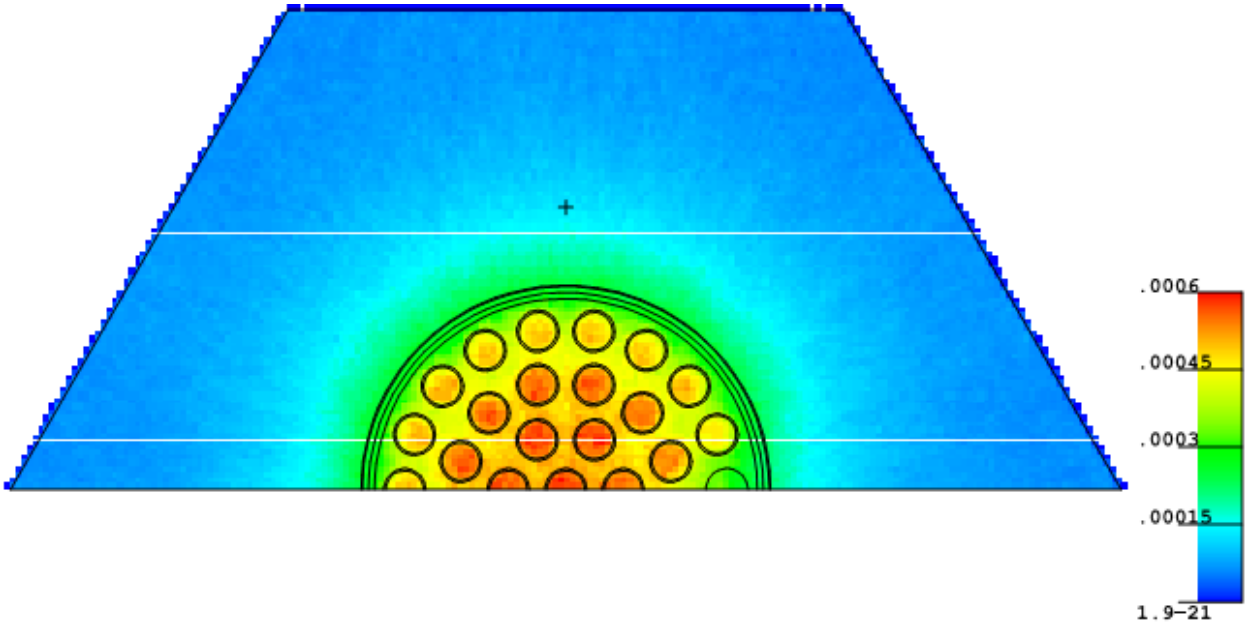

Figure 3-4. MCNP fast energy group (1-20 MeV) neutron flux tally.

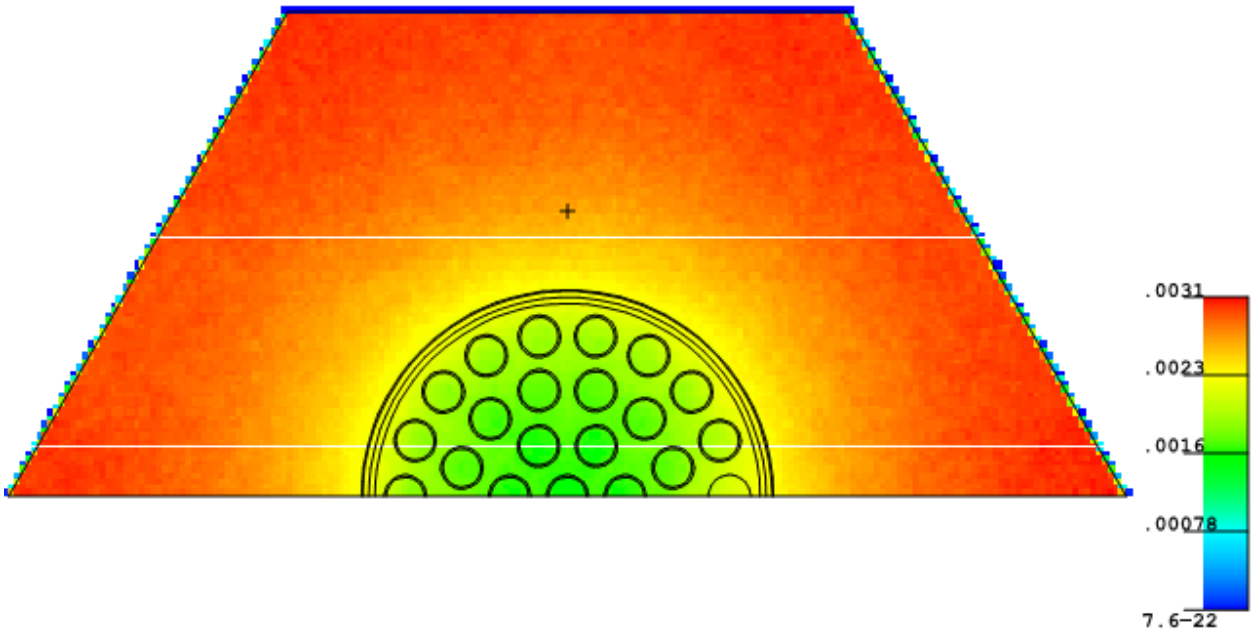

Figure 3-5. MCNP thermal energy group (0-0.175 eV) neutron flux tally.

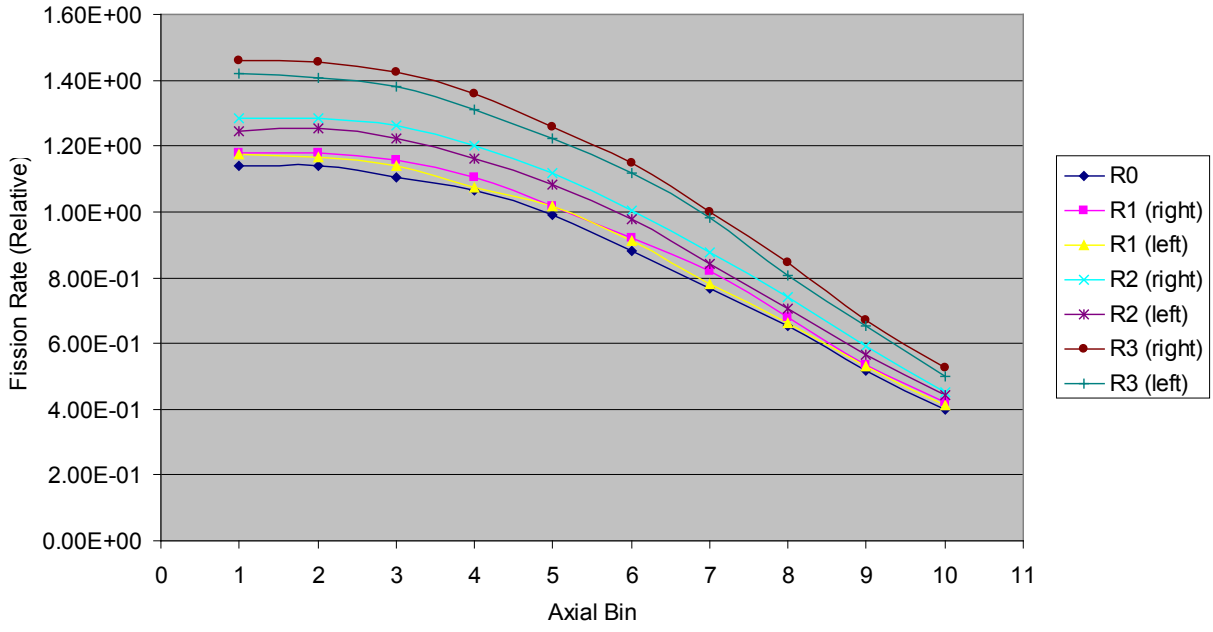

Figure 3-6. Assembly fission rate by pin and axial zone. R represents the radial position of the pin in the assembly (0-3). Left and right pins are the leftmost and rightmost pins as shown in Figure 3-2.

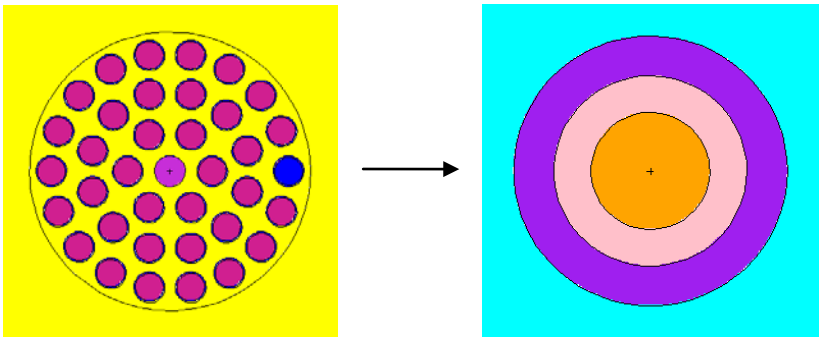

Figure 3-7. Non-homogenized and homogenized versions of a fuel assembly.

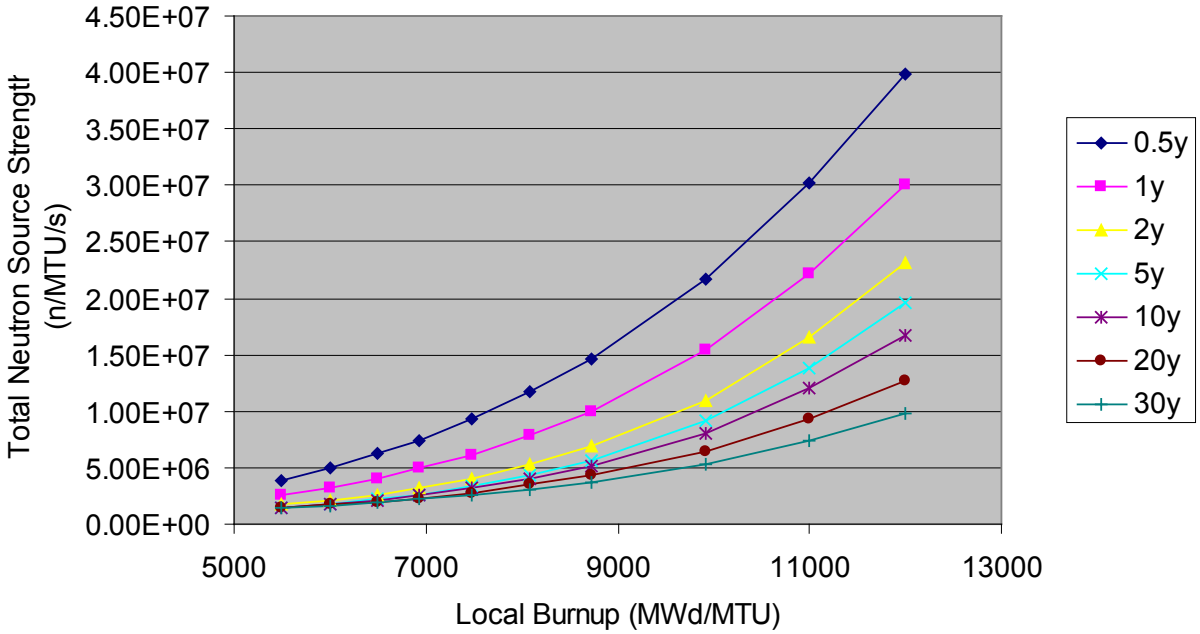

Figure 3-8. Total neutron source strength as a function of local burnup for NU fuel based on ORIGEN-ARP point depletion calculation.

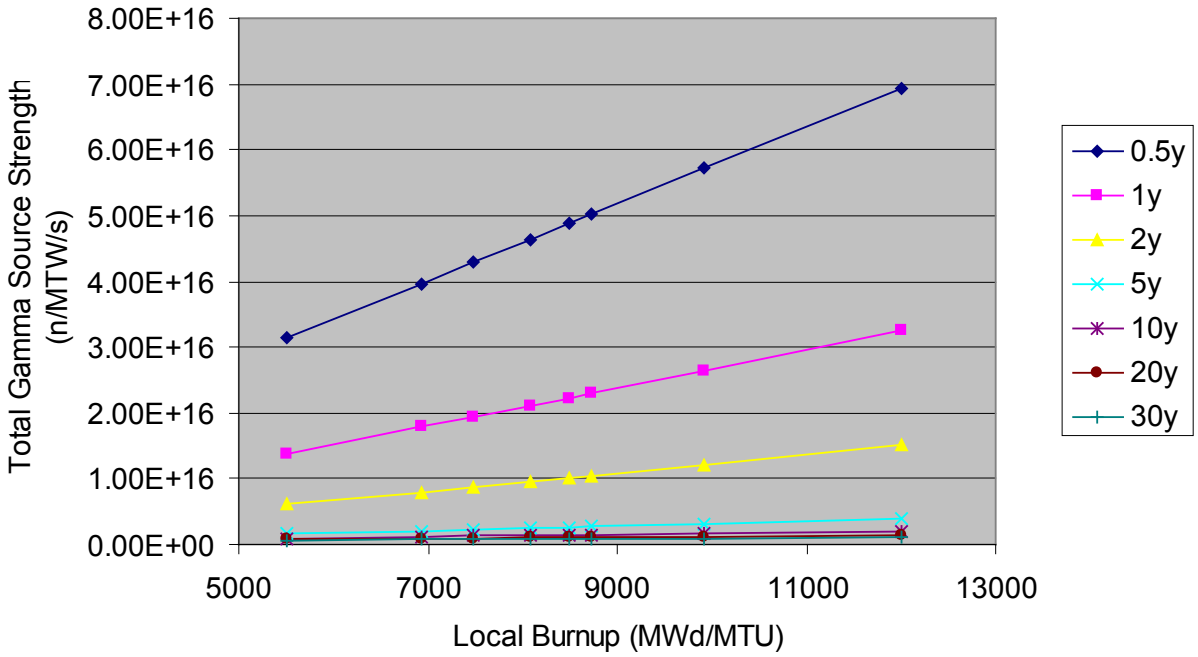

Figure 3-9. Total gamma source strength as a function of local burnup for NU fuel based on ORIGEN-ARP point depletion calculation.

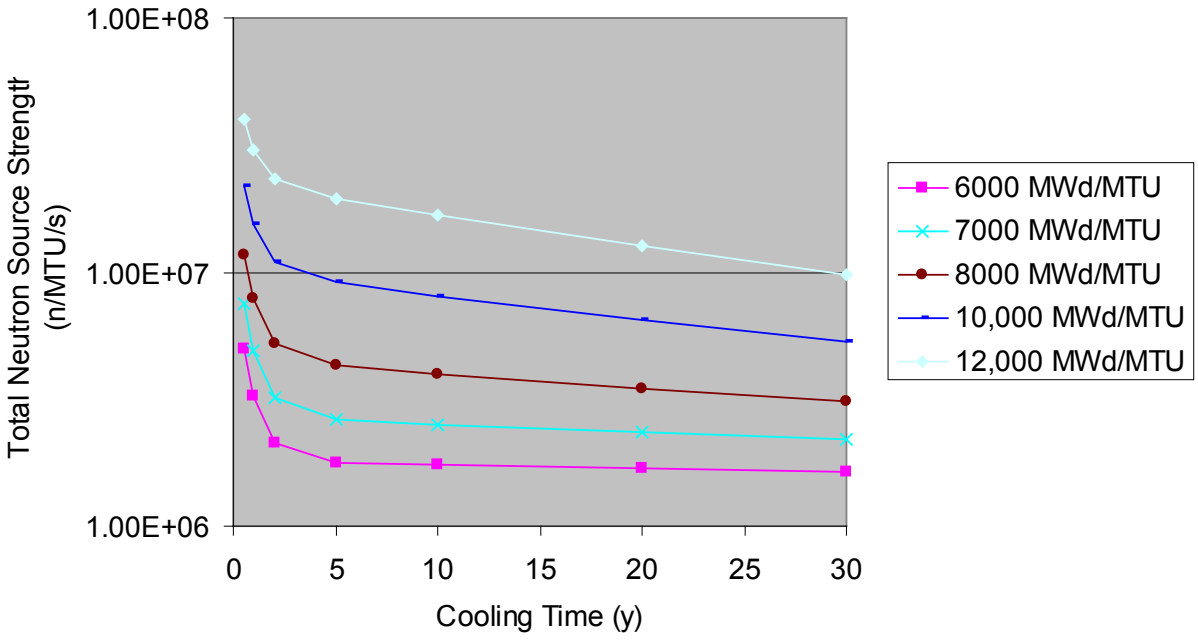

Figure 3-10. Total neutron source strength as a function of decay time for NU fuel based on ORIGEN-ARP point depletion calculation.

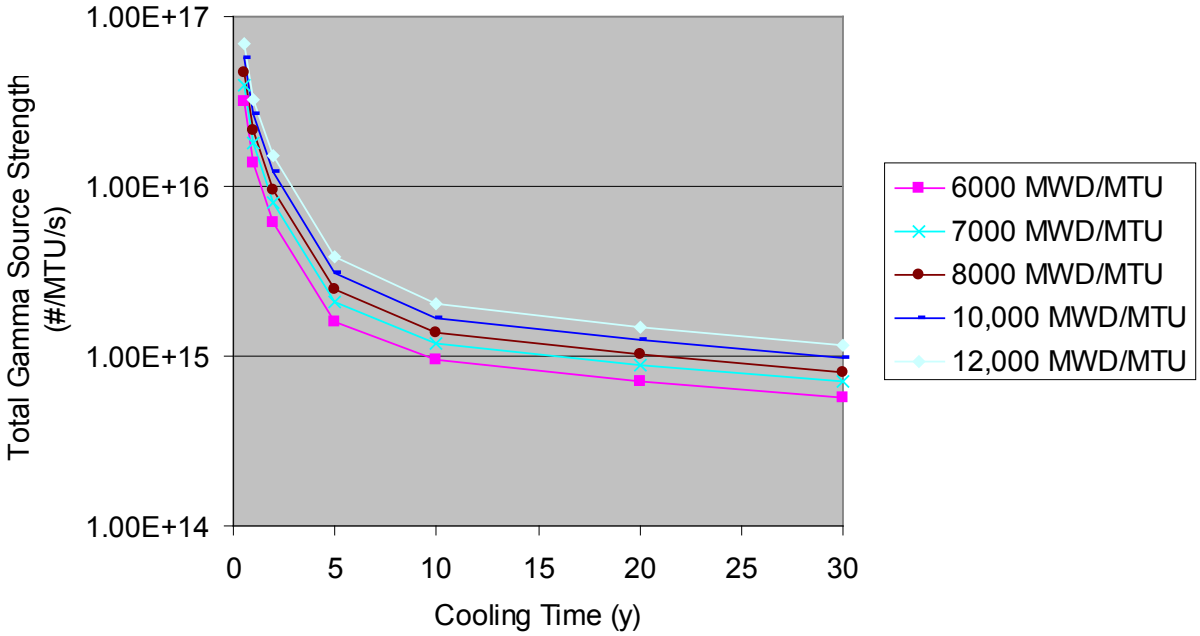

Figure 3-11. Total gamma source strength as a function of decay time for NU fuel based on ORIGEN-ARP point depletion calculation.

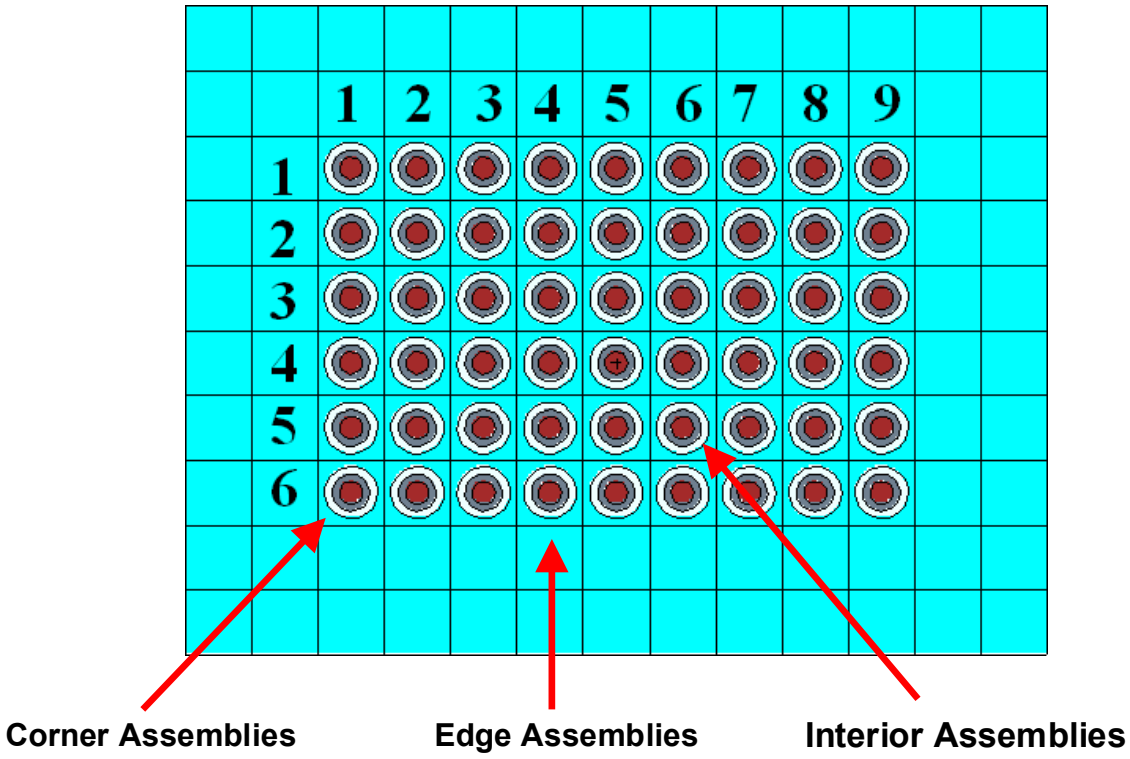

Figure 3-12. MCNP model of the spent fuel pool showing examples of corner, edge and interior assemblies.

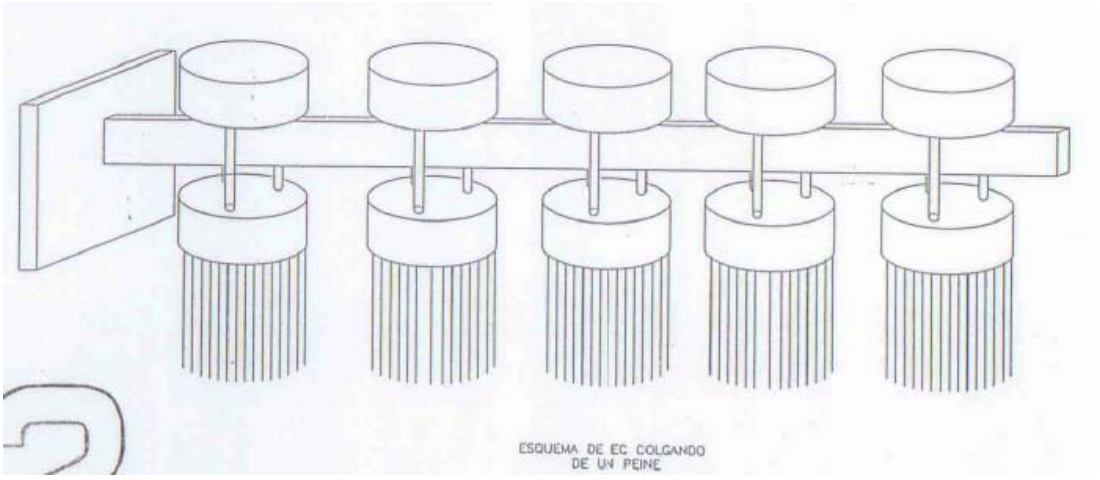

Figure 3-13. Side view diagram of the Atucha-I spent fuel storage

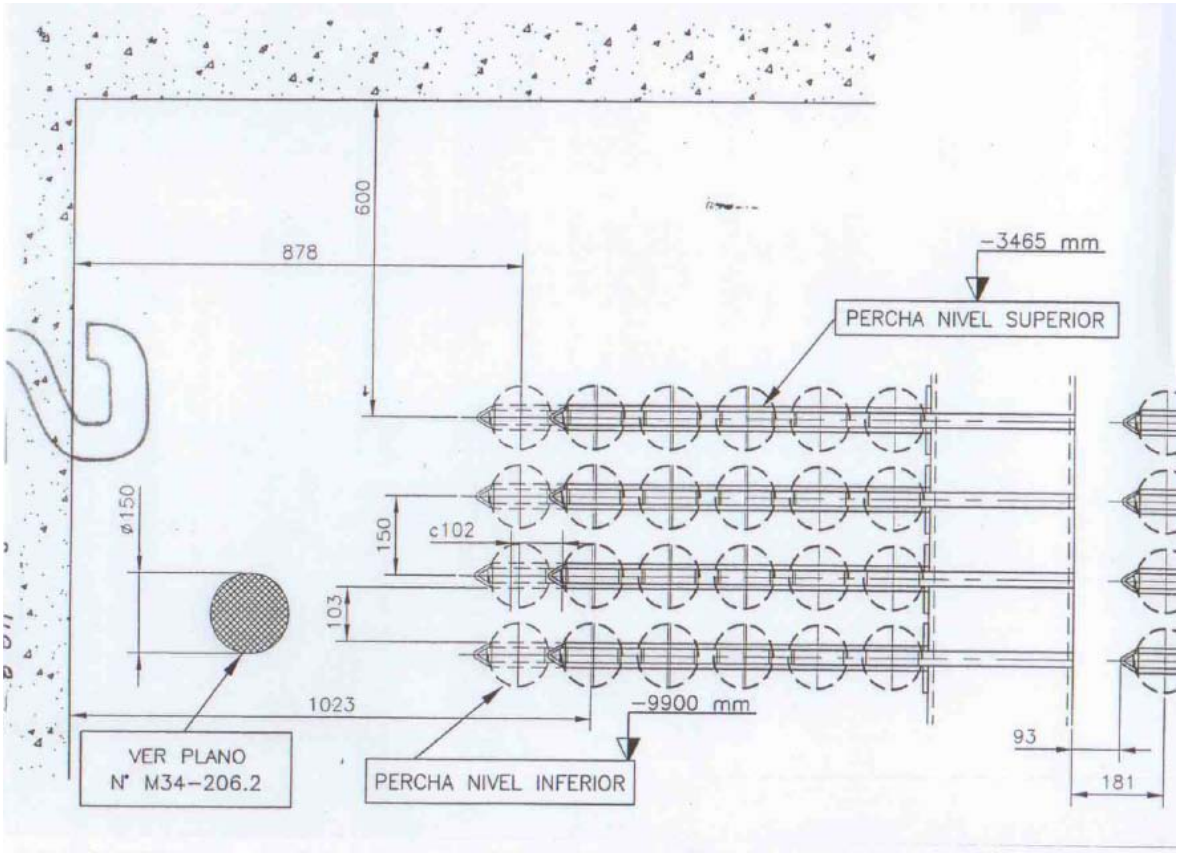

Figure 3-14. Top view diagram of the Atucha-I spent fuel storage

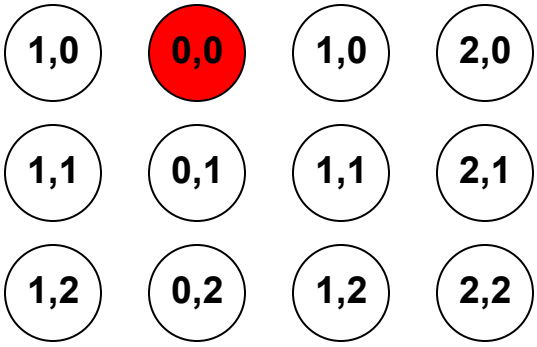

Figure 3-15. Positions of assemblies relative to the source assembly (red)

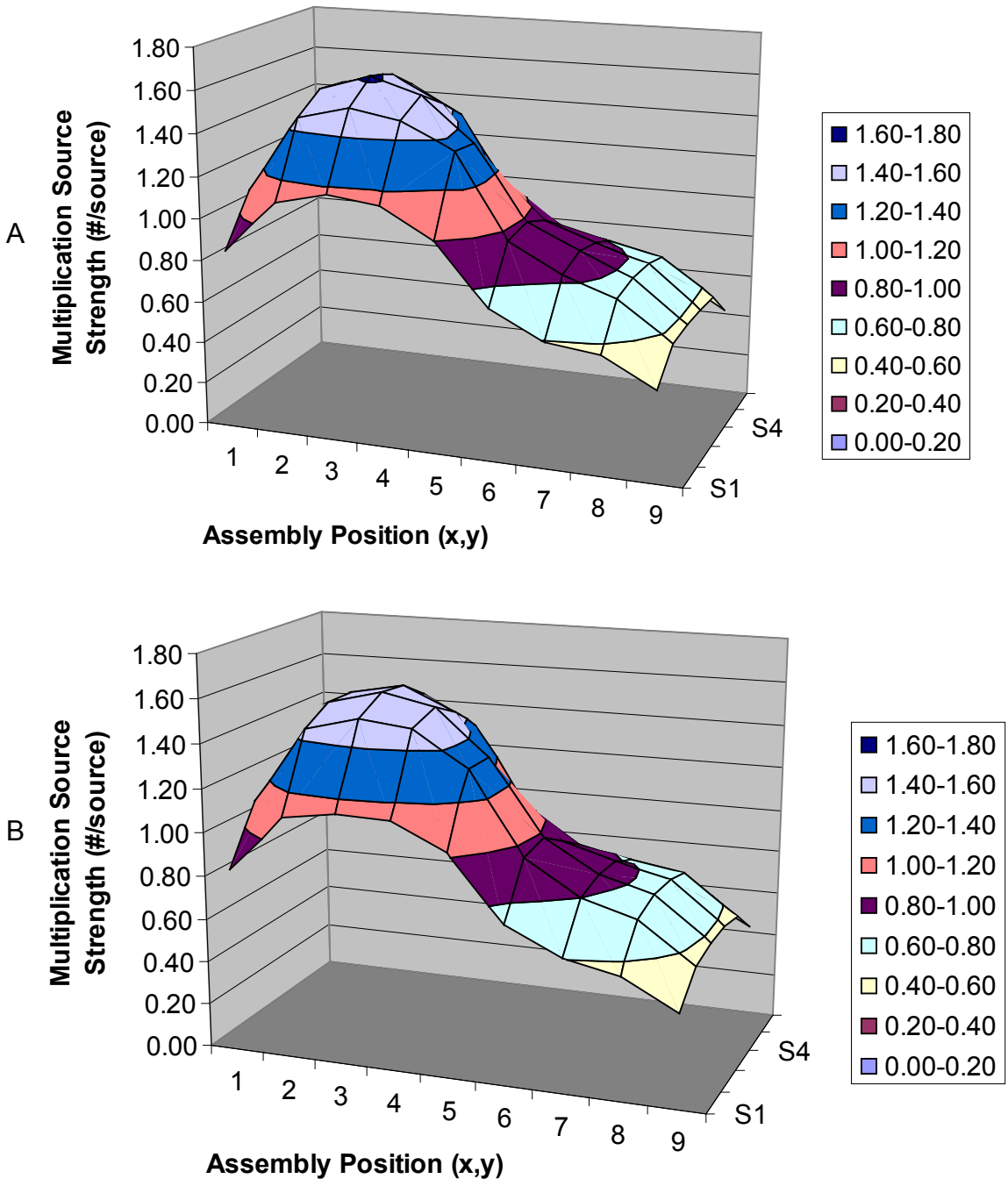

Figure 3-16. Calculated multiplication source by assembly for the 9x6 non-uniform source arrangement. A) Using MCNP. B) Using the fission-matrix method.

A

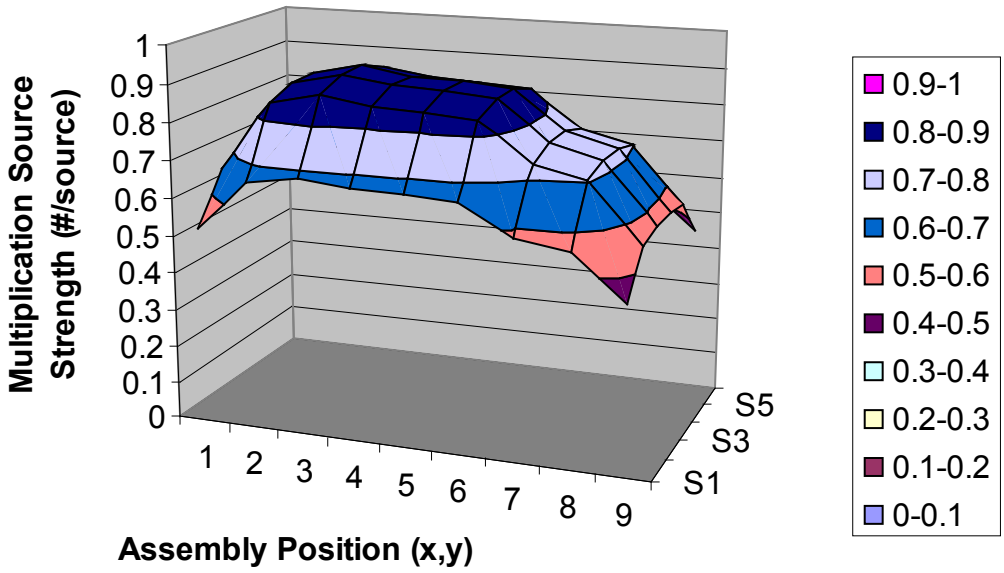

B

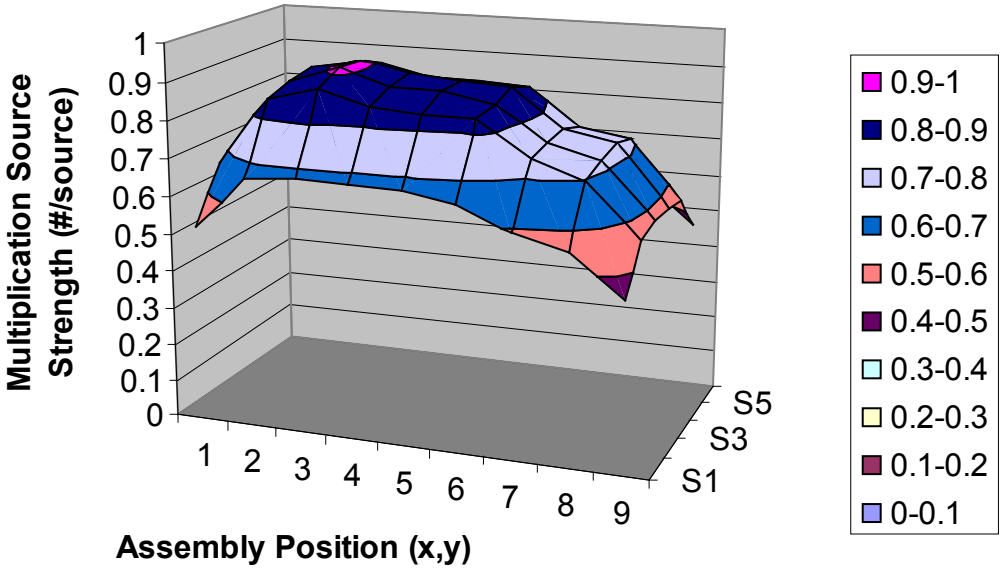

Figure 3-17. Calculated multiplication sources by assembly for a 9x6 array with three 3x6 regions of different burnup and decay times. A) Using MCNP B) Using the fission-matrix method.

Table 3-1. Atucha-I Detailed Properties

Reactor Property	Value
Thermal Power (MW)	1179
Electrical Power (MW)	357
Moderator/Coolant Flow/Reflector	D2O (99.9%)
Primary Coolant Inlet/Outlet Temp (°C):	265/299 (280 avg)
Average Moderator Temperature (°C):	190
D2O Coolant and Moderator Pressure (MPa):	11.3
Coolant Density (g/cc)	0.838
Moderator Density (g/cc)	0.979
Channel Lattice	Hexagonal
Lattice Pitch (mm)	272
Coolant Tube ID (mm)	108.2
Coolant Tube Thickness (mm)	1.72
Moderator Isolation Distance (mm)	1.7
Isolation Tube Thickness (mm)	0.4
Cladding Material	Zircaloy 4
Coolant Tube Material	Zircaloy 2
UO2 Pellet diameter (mm)	10.7
UO2 Density (g/cc)	10.5
Clad Outside Diameter (mm)	11.9
Clad Thickness (mm)	0.55
Clad Material	Zircaloy 4
Uranium Enrichment – Old (w%)	0.711 (NU)
Uranium Enrichment – New (w%)	0.850 (SEU)
Active Fuel Length	5300
Number of Fuel Rods	36
Number of Structural Pins	1

Table 3-2. Local Burnup to Average Burnup Ratio for Assembly Burnup Zones

	Radial Zone			
Axial Zone	1	2	3	All
1	1.16	1.25	1.42	1.30
2	1.08	1.17	1.33	1.22
3	1.01	1.09	1.23	1.13
4	0.91	0.99	1.12	1.03
5	0.79	0.86	0.97	0.89
6	0.67	0.72	0.82	0.75
7	0.53	0.57	0.65	0.60
8	0.41	0.45	0.50	0.46
All	0.89	0.96	1.09	1.00

Table 3-3. Principle Neutron Source Isotopes for NU Fuel at 7000 MWd/MTU

Reaction Type	Isotope	Neutron Source Strength (n/MTU/s) Decay Time 1 y	2 y	5 y	10 y	20 y	30 y
(α,n)	Pu-238	5.39E+04	5.45E+04	5.35E+04	5.14E+04	4.75E+04	4.39E+04
(α,n)	Pu-239	9.82E+04	9.82E+04	9.82E+04	9.82E+04	9.82E+04	9.81E+04
(α,n)	Pu-240	1.35E+05	1.35E+05	1.35E+05	1.35E+05	1.35E+05	1.35E+05
(α,n)	Am-241	3.19E+04	5.58E+04	1.21E+05	2.10E+05	3.31E+05	4.03E+05
(α,n)	Cm-242	3.67E+05	7.79E+04	1.05E+03	3.03E+02	2.88E+02	2.75E+02
(α,n)	Cm-244	1.07E+04	1.03E+04	9.19E+03	7.59E+03	5.17E+03	3.53E+03
Spontaneous Fission (SF)	U-238	1.34E+04	1.34E+04	1.34E+04	1.34E+04	1.34E+04	1.34E+04
(SF)	Pu-238	1.03E+04	1.04E+04	1.02E+04	9.81E+03	9.07E+03	8.38E+03
(SF)	Pu-240	9.90E+05	9.90E+05	9.89E+05	9.89E+05	9.88E+05	9.87E+05
(SF)	Pu-242	8.79E+04	8.79E+04	8.79E+04	8.79E+04	8.79E+04	8.79E+04
(SF)	Cm-242	1.92E+06	4.08E+05	5.47E+03	1.59E+03	1.51E+03	1.44E+03
(SF)	Cm-244	1.51E+06	1.46E+06	1.30E+06	1.07E+06	7.30E+05	4.98E+05
(SF)	SUM	5.23E+06	3.40E+06	2.82E+06	2.67E+06	2.45E+06	2.28E+06
(SF)	TOTAL	5.23E+06	3.40E+06	2.82E+06	2.68E+06	2.45E+06	2.28E+06

Table 3-4. Fission Matrix Coefficients for an Interior NU Assembly Calculated Using MCNP

	Fission Matrix Coefficients[a] x-distance from source assembly		
y-distance	0	1	2
0	2.13E-01	4.98E-02	2.70E-03
1	4.56E-02	1.38E-02	1.22E-03
2	2.18E-03	1.11E-03	

[a]Monte Carlo relative uncertainties <1%

Table 3-5. Fission Matrix Coefficients for an Edge NU Assembly Calculated Using MCNP

	Fission Matrix Coefficients[a] x-distance from source assembly		
y-distance	0	1	2
0	2.14E-01	4.98E-02	2.69E-03
1	4.57E-02	1.37E-02	1.22E-03
2	2.17E-03	1.08E-03	

[a]Monte Carlo relative uncertainties <1%

Table 3-6. Fission Matrix Coefficients for a Corner NU Assembly Calculated Using MCNP

	Fission Matrix Coefficients[a]		
	x-distance from source assembly		
y-distance	0	1	2
0	2.15E-01	5.00E-02	2.66E-03
1	4.58E-02	1.38E-02	1.22E-03
2	2.17E-03	1.08E-03	

[a]Monte Carlo relative uncertainties <1%

Table 3-7. Multiplication Factors using MCNP and Fission Matrix

Assembly Arrangement	M (MCNP)	M (Fission Matrix)	Difference	MCNP Uncertainty [a]
2x6, uniform	1.7133	1.7104	-0.0029	0.0008
9x6, uniform	1.9988	1.9966	-0.0022	0.0007
9x6, non-uniform	2.0033	1.9968	-0.0065	0.0013
20x6, uniform	2.0513	2.0444	-0.0069	0.0012

[a]1-sigma statistical uncertainty

CHAPTER 4
DETECTOR IMPORTANCE AND FIELD-OF-VIEW (FOV)

In this Chapter, we determine the detector FOV using the PENTRAN 3-D Sn transport code system and compare its results to the Monte Carlo MCNP predictions. To develop an efficient model, we perform various sensitivity analyses for the PENTRAN calculations.

4.1 PENTRAN Model for Determination of the Detector FOV

A 2D model was created using PENTRAN to evaluate the detector importance. The detector was a 2.54 cm diameter fission chamber surrounded by a 6 cm diameter polyethylene moderator. Figure 4-1 shows a diagram of the neutron detector used at Atucha-I. The model consists of the detector surrounded by sixteen fuel assemblies in water. Only one quarter of the model is simulated by using reflective boundary conditions. Two assembly spacing arrangements used at Atucha-I were tested: 14.5 cm in the x direction and 15.0 cm in the y direction for the NU fuel, and 13.5 cm in both directions for the SEU fuel. The PENTRAN model of the SEU arrangement is shown in Figure 4-2. The PENMSHXP utility was used to create the mesh structure[12]. See Appendix D for the PENTRAN input file.

4.1.1 Cross Sections and Adjoint Source

Cross sections for performing transport calculations were taken from the BUGLE-96 library[13], with 47 neutron groups and 20 photon groups. The neutron energy group boundaries are shown in Table 4-1. The GMIX utility[14] was used to mix the cross sections of materials calculated in Chapter 3. Cooling time for the materials was assumed to be 10 years. It will be shown later that both cooling time and burnup do not have a large effect on the cross-section values.

In order for the calculation to yield a proper detector importance, the adjoint source must be equal to the cross-section of the detector of interest. In this case, the detector is a fission chamber using 94 w% enriched U. So, the fission cross-section of 94% enriched U was used as the adjoint source. Detailed detector specifications are given in Table 4-2. A graph of the detector cross-section (or adjoint source) is shown in Figure 4-3.

4.1.2 Spatial Meshing and Angular Quadrature

In order to test for proper convergence, several calculations with different mesh sizes and quadrature orders must be tested. This was performed for mesh sizes of 0.135 cm and 0.270 cm; angular quadrature sets tested were S4 and S8. For these cases, the fractional response of each detector was calculated, assuming identical sources in all assemblies. Results are shown in Table 4-3, which shows almost identical results for the cases tested, indicating that a fine mesh size of 0.270 cm and S4 quadrature should be adequate.

4.1.3 Effect of Model Size and Assembly Burnup

Next, calculations were performed to determine the impact of changing the size of the model. A model with 9 surrounding assemblies (i.e., 3x3) instead of 4 assemblies was created, to see if extra assemblies are needed. Another calculation was performed using cross sections from fresh fuel in order to see the impact of burnup and/or cooling time on the FOV. The resulting FOVs are presented in Table 4-4.

Expanding the model from 2x2 to 3x3 resulted in only ~1% increased response. This was deemed to be insignificant for our purposes. The fresh fuel numbers are also very close, especially given the very large difference of burnups (0 MWd/MTU vs 11000 MWd/MTU). This indicates that any differences in assembly burnup can be ignored in

terms of cross sections, especially in the comparatively small range of burnups that will be encountered (9000-13000 MWD/MTU for SEU Fuel).

4.1.4 3D PENTRAN Model

A 3D model was created to make sure that there was not a large effect due to the finite axial detector size. The 3D model is shown in Figure 4-4. The active portion of the detector is in red, the inactive portion is in pink, the polyethylene is in orange and a tungsten shield (to shield electronics) is in white. Top, bottom, +x and +y directions had vacuum boundaries while –x, -y had reflective conditions.

Figure 4-5 shows the importance function for adjoint group 30, which represents the approximate midpoint of the source spectrum (1.0-1.35 MeV). FOV results from the 3D calculation are given in Table 4-5. The FOV is almost identical, indicating that a 2D model is adequate to represent the problem while requiring much less computational effort. In the z-direction, the importance profile shows that 90% of the response comes from a ~30cm axial region surrounding the detector. This indicates that the axial FOV extends only in the first axial burnup zone (that is 159cm in length).

4.1.5 Effect of Neutron Spectrum on FOV

If the spectrum of neutrons is changed significantly with burnup or cooling time, then the resulting FOV could change due to a different source term. To check this, the importance was coupled with sources with different cooling times and burnups, presented in Table 4-6. Results indicate that there is very little spectral difference for changing cooling times and burnups. Results are for the NU fuel arrangement; hence, the difference between assemblies 2 and 3 due to different pitches in each direction.

4.1.6 Edge Effect on the Detector FOV

So far, these results have been for a detector placed somewhere in the middle of the pool where it is surrounded by assemblies. We now examine the impact on the FOV if the detector is placed on the edge of the spent fuel array. The model examined is shown in Figure 4-6. The detector is in light blue and the fuel assemblies are yellow-green. The boundaries are reflective in –y and vacuum on all others. Results are shown in Table 4-7. Positioning the detector at the edge of the array shows a slight shift in the FOV from assembly 2 to assembly 3, due to less absorption in the vicinity of 3. The total response is also increased by about 5%. Depending on the required accuracy of the system, this response shift may need to be taken into account.

4.2 Monte Carlo Calculation of FOV and Comparison

In order to benchmark the above deterministic importance function results, a forward Monte Carlo transport calculation was performed using MCNP. The model used can be seen in Figure 4-7. The yellow and blue circles designate the detector. The numbered assemblies represent the source location for each of four calculations.

Flux was tallied in the detector and multiplied by the fission cross-section of the detector (94 w% U-235). This tally was compared for the four different source locations and the FOV was calculated. These results are compared to the PENTRAN results in Table 4-8. As expected, above results indicate excellent agreement between the "forward" Monte Carlo MCNP calculations and the adjoint deterministic PENTRAN calculations.

4.3 Determination of the Gamma detector FOV

The FOV of a gamma detector was also investigated. Since there is a wide range of detector possibilities, here we consider a detector which is uniformly sensitive to all

energies. The model used was identical to the neutron detector model except for the adjoint source (uniform). Using a 2-D PENTRAN model, a coupled neutron and gamma calculation was performed to determine the importance of both gammas and neutrons, through (n,γ) reactions, for a gamma detector in the same geometry as for the neutron detector. FOV results for different cooling times are shown in Table 4-9. The FOV changes very slightly due to a shift in energy spectrum as source isotopes decay. Different burnups were not tested due to the linear nature of the gamma source with burnup (see Figure 3-8).

As expected, the results indicate that the gamma response from neutrons due to (n,γ) reactions was negligible as compared to the direct decay gammas. Also, the FOV was somewhat skewed toward the detector, because of the more limited range of the lower energy gammas compared to neutrons.

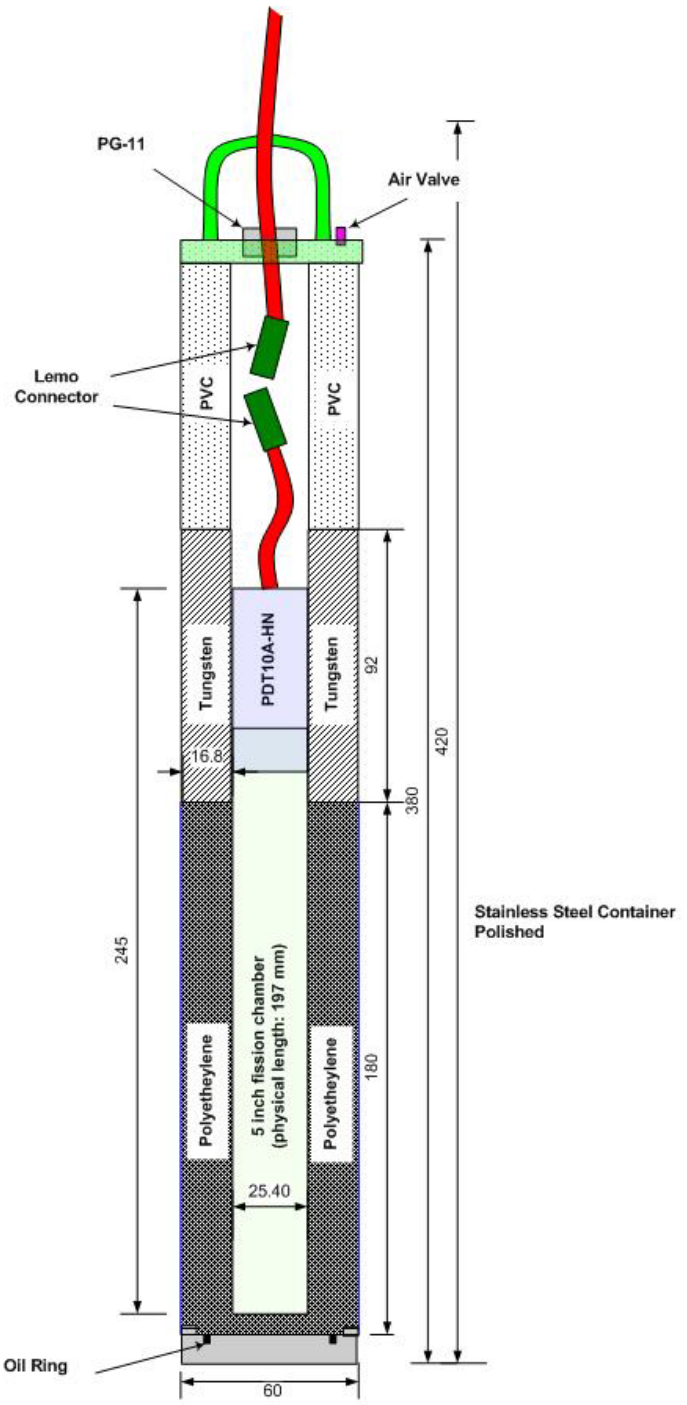

Figure 4-1. Diagram of the fission chamber detector used at Atucha (dimensions in mm)

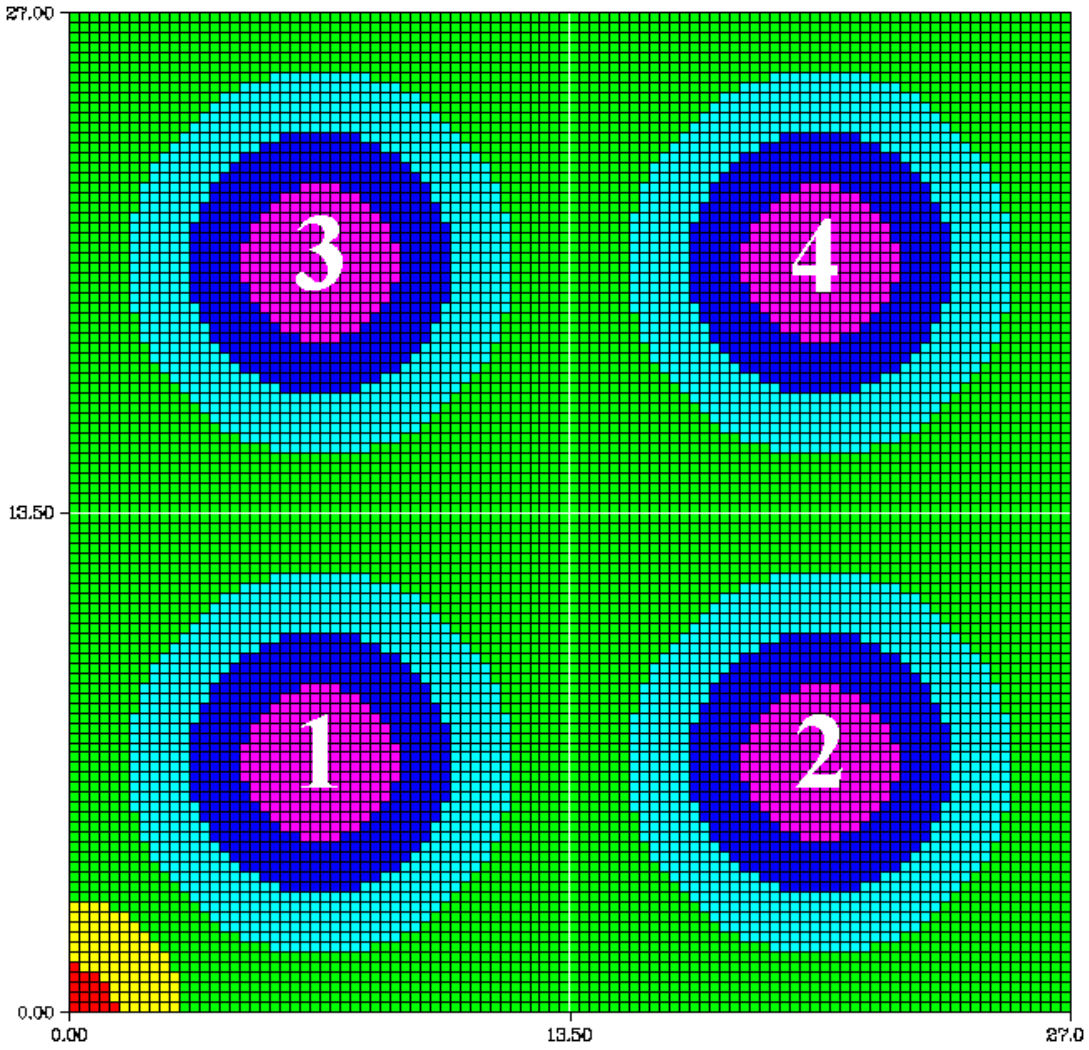

Figure 4-2. 2D model of the SEU spent fuel pool in PENTRAN. The detector is in red at the bottom left corner. Assembly numbers are also shown.

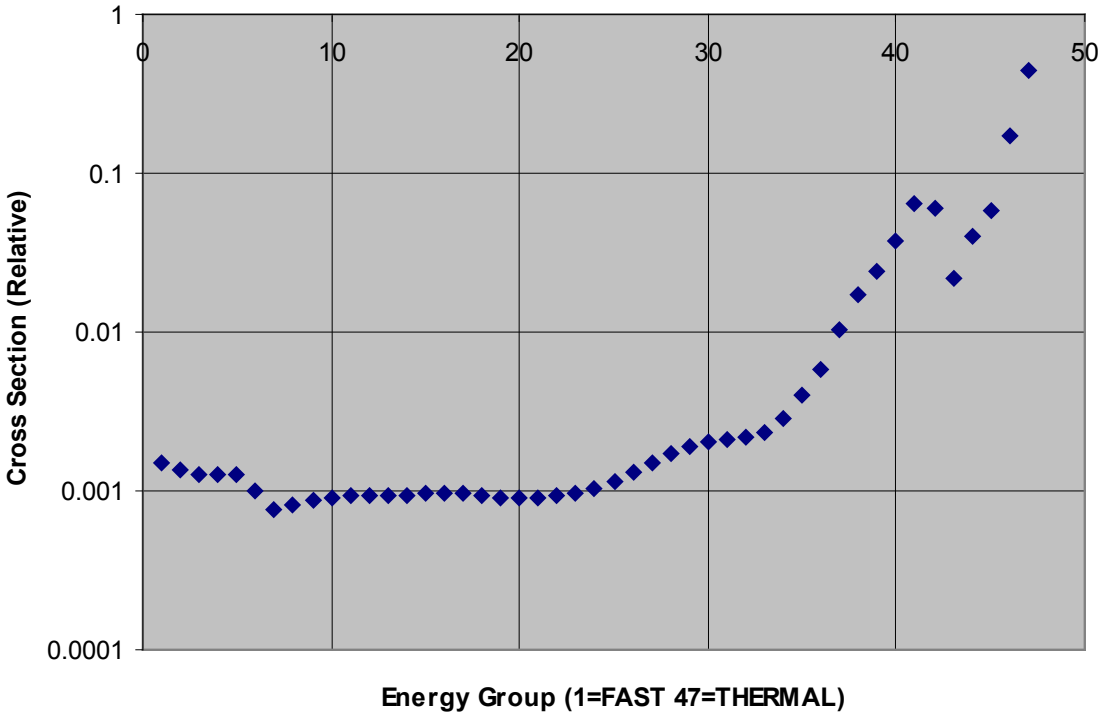

Figure 4-3. Fission chamber detector cross-section (or adjoint source)

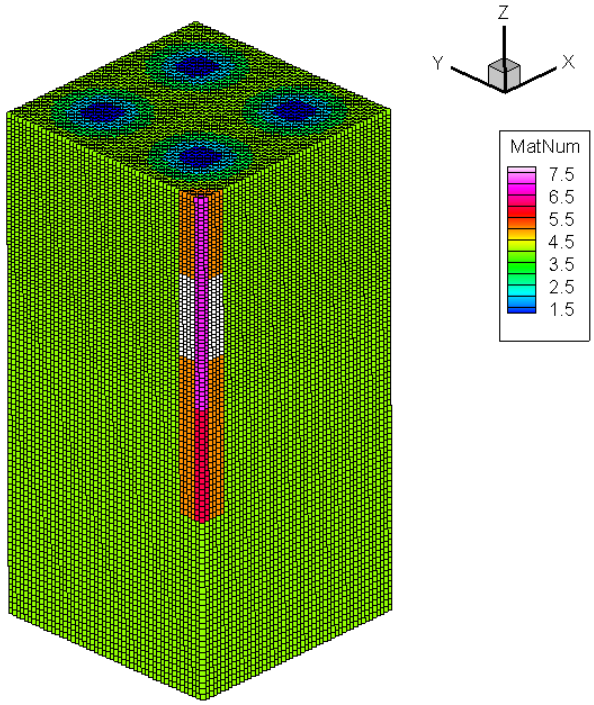

Figure 4-4. 3D model of detector and spent fuel pool in PENTRAN. In red is the active portion of the detector.

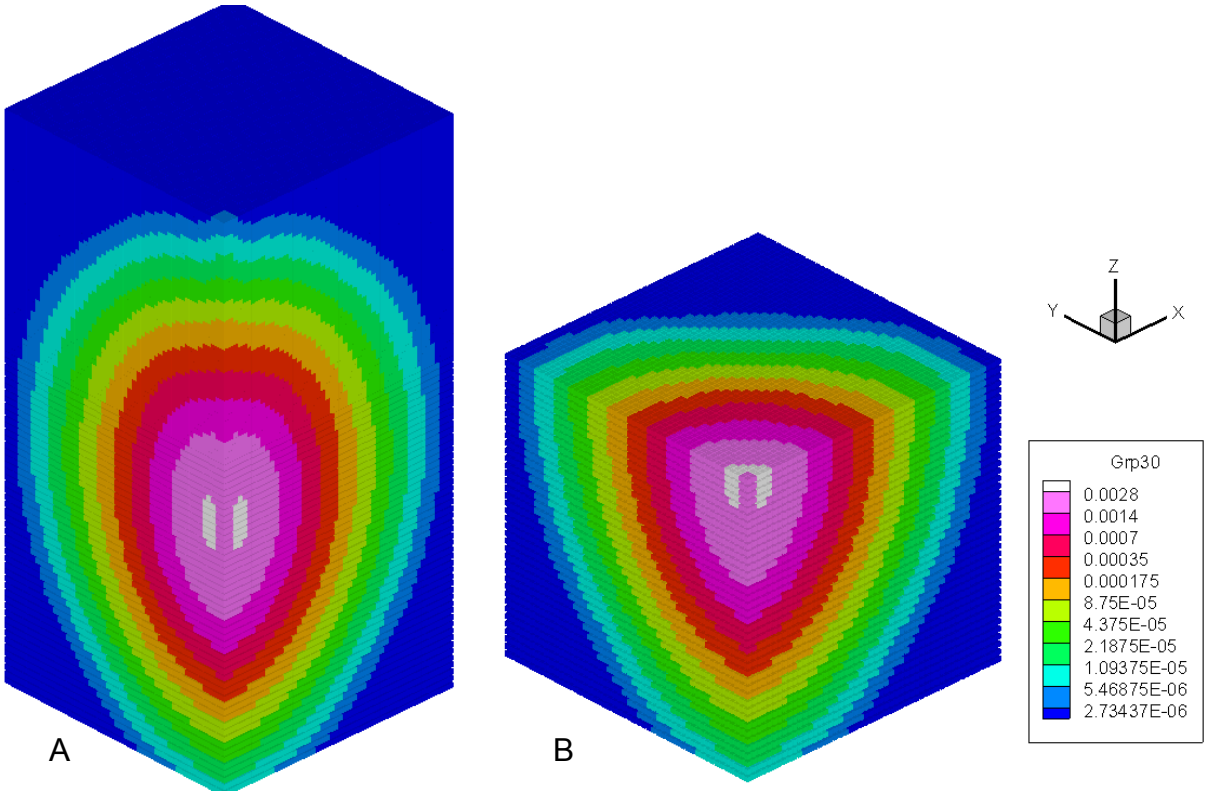

Figure 4-5. Adjoint group 30 (1-1.35 MeV) neutron importance profile for 3D PENTRAN model. The scale is logarithmic. A) Full model B) Slice in the Z plane.

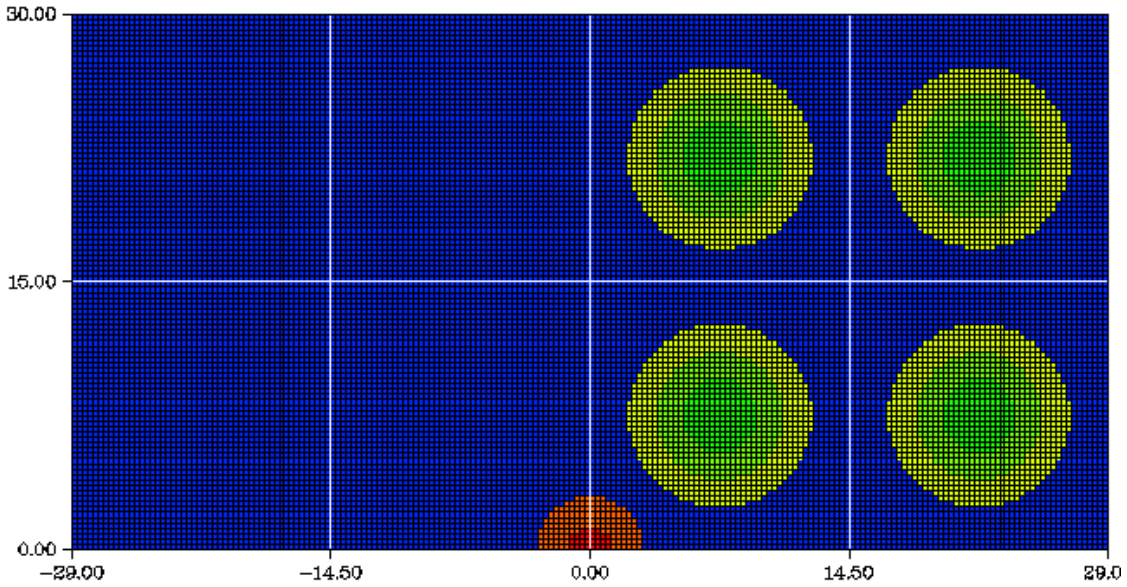

Figure 4-6. 2D PENTRAN model of a detector (orange-red) at the edge of the spent fuel array (yellow-green). The model is reflected in the –y direction and vacuum boundaries elsewhere.

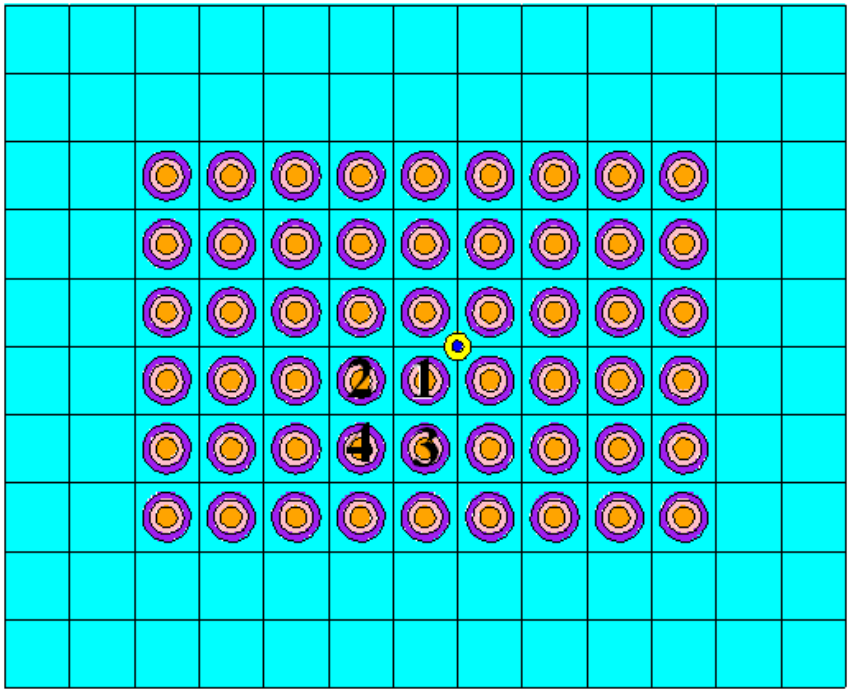

Figure 4-7. MCNP spent fuel and detector model with detector shown in blue and yellow.

Table 4-1. BUGLE-96 Energy Group Structure

Energy Group Number	Lower Bound (MeV)	Upper Bound (MeV)
47	1.00E-11	1.00E-07
46	1.00E-07	4.14E-07
45	4.14E-07	8.76E-07
44	8.76E-07	1.86E-06
43	1.86E-06	5.04E-06
42	5.04E-06	1.07E-05
41	1.07E-05	3.73E-05
40	3.73E-05	1.01E-04
39	1.01E-04	2.14E-04
38	2.14E-04	4.54E-04
37	4.54E-04	1.58E-03
36	1.58E-03	3.35E-03
35	3.35E-03	7.10E-03
34	7.10E-03	1.50E-02
33	1.50E-02	2.19E-02
32	2.19E-02	2.42E-02
31	2.42E-02	2.61E-02
30	2.61E-02	3.18E-02
29	3.18E-02	4.09E-02
28	4.09E-02	6.74E-02
27	6.74E-02	1.11E-01
26	1.11E-01	1.83E-01
25	1.83E-01	2.97E-01
24	2.97E-01	3.69E-01
23	3.69E-01	4.98E-01
22	4.98E-01	6.08E-01
21	6.08E-01	7.43E-01
20	7.43E-01	8.21E-01
19	8.21E-01	1.00E+00
18	1.00E+00	1.35E+00
17	1.35E+00	1.65E+00
16	1.65E+00	1.92E+00
15	1.92E+00	2.23E+00
14	2.23E+00	2.35E+00
13	2.35E+00	2.37E+00
12	2.37E+00	2.47E+00
11	2.47E+00	2.73E+00
10	2.73E+00	3.01E+00
9	3.01E+00	3.68E+00
8	3.68E+00	4.97E+00
7	4.97E+00	6.07E+00
6	6.07E+00	7.41E+00
5	7.41E+00	8.61E+00
4	8.61E+00	1.00E+01
3	1.00E+01	1.22E+01
2	1.22E+01	1.42E+01
1	1.42E+01	1.96E+01

Table 4-2. Fission Chamber Detector Specifications

Detector Type	RS-P6-0805-134 Fission Chamber
Diameter	2.54 cm
Active Length	12.7 cm
Active Material	93% enriched U-235
Total U-235	12 mg
Fill Gas	Argon/Nitrogen (760 torr)
Casing Material	Aluminum

Table 4-3. Fractional Response of Assemblies for Varying Mesh Size and Quadrature (SEU Fuel)

Fine Mesh Size (cm)	Quadrature Order	Assembly # 1	2	3	4
0.270	S4	86.55%	6.13%	6.13%	1.19%
0.270	S8	86.74%	5.99%	5.99%	1.27%
0.135	S4	86.56%	6.13%	6.13%	1.19%
0.135	S8	86.75%	5.99%	5.99%	1.27%

Table 4-4. Fractional Response for Different Model Size and Cross Sections

	Assembly Identification Number				
Assembly Arrangement	1	2	3	4	Sum of 5-9
2x2	86.74%	5.99%	5.99%	1.27%	N/A
3x3	85.72%	5.94%	5.94%	1.21%	1.18%
2x2 (Fresh Fuel)	85.63%	6.52%	6.52%	1.33%	N/A

Table 4-5. Comparison of FOV for 2D and 3D models (SEU Fuel)

Assembly Number	FR_i *(3D)	FR_i (2D)
1	86.75%	86.74%
2	6.05%	5.99%
3	6.05%	5.99%
4	1.14%	1.27%

*Fractional Response of Assembly *i* to detector

Table 4-6. FOV Variation with Fuel Burnup and Cooling Time (NU Fuel)

Average Burnup (MWd/MTU)	Cooling Time (years)	Assembly Identification Number 1	2	3	4
5000	10	88.65%	5.31%	5.15%	0.90%
8000	10	88.66%	5.29%	5.14%	0.92%
6000	1	88.54%	5.34%	5.19%	0.93%
6000	30	88.47%	5.39%	5.23%	0.91%

Table 4-7. Relative Assembly Importance in PENTRAN and MCNP (NU Fuel)

Assembly #	PENTRAN FOV	MCNP FOV	MCNP Uncertainty
1	88.55%	87.43%	0.0026%
2	5.35%	6.29%	0.45%
3	5.20%	5.18%	0.59%
4	0.91%	1.10%	6.1%

Table 4-8. Comparison of Detector Response for Interior and Edge Locations

	Fractional Response by Assembly				Total Response
Detector Location	1	2	3	4	(Ratio)
Interior	88.40%	5.43%	5.27%	0.91%	1.000
Edge	88.21%	5.36%	5.51%	0.91%	1.047

Table 4-9. FOV of Uniform Gamma Detector (NU Fuel)

	Assembly Number				$\frac{(n,\gamma)}{(n,\gamma)+Decay\,\gamma}$
Cooling Time (years)	1	2	3	4	
1	88.11%	6.26%	5.06%	0.57%	5.58E-09
5	88.75%	5.97%	4.77%	0.51%	1.83E-08
20	89.02%	5.85%	4.65%	0.48%	3.12E-08

CHAPTER 5
DETECTOR RESPONSE PREDICTION

Based on the results of previous sections, we developed the following procedure for the determination of detector response:

- Prepare the assembly array properties (arrangement, burnup and cooling time)
- Determine the intrinsic sources in each assembly and radial zone by interpolating the source database
- Use the geometry and intrinsic source to calculate the multiplication source for each assembly using the fission matrix method
- Use the detector importance function with the total source to determine the hypothetical detector response for various detector locations and detector types.

The detector response at each location is calculated by Equation 5-1.

$$R_i = \sum_{j=1}^{N} \sum_{g=1}^{G} \Psi^*_{i,j,g} S_{j,g} \qquad (5\text{-}1)$$

Where R_i denotes the response of the detector at location i. $\Psi^*_{i,j,g}$ is the importance of particles in energy group g in assembly j for a detector at i. $S_{j,g}$ is the source strength at assembly j in energy group g. $\Psi^*_{i,j,g}$ is assumed to be identical for all i's except for a translation to center Ψ^* about each detector location (i.e. distance from the detector to the assembly is the important variable). This ignores any changes in Ψ^* due to effects near the edge of the assembly array, which were previously determined to be small. If additional accuracy is required, corrections could be made to Ψ^* at the edge of the pool.

5.1 Estimation of Detector Efficiency

Due to unknown detector efficiency, the calibration data is needed to obtain meaningful numbers. The efficiency is estimated by minimizing the square error of the estimate given by Equation 5-2.

$$\varepsilon = \sum_i (Ex_i - r_i)^2 \tag{5-2}$$

Where, x_i is the raw estimated response at location i, r_i is the experimental response at location i, E is the detector effiency and ε is the sum of the square error.

If ε is minimized (i.e. setting $d\varepsilon/dE = 0$) then the estimated efficiency is recovered by Equation 5-3.

$$E = \frac{\sum_i x_i r_i}{\sum_i x_i^2} \tag{5-3}$$

If no proper calibration data is available, then relative numbers can be obtained by arbitrarily setting one data point equal to one.

5.2 Response Error due to Burnup Uncertainty

There will be an error in the calculated detector responses due to uncertainty in the burnup of the fuel assemblies. As determined earlier, a change of burnup has little effect on the importance function and detector field of view. It will, however, have a large effect on the source, which has a direct impact on the detector response. The response error due to burnup uncertainty is calculated using standard error propagation.

R_i, the total detector response at location i, is equal to the sum of the responses due to the sources located in all assemblies as shown in Equation 5-5.

$$R_i = \sum_{j=1}^{N} r_{i,j}(BU_j) \tag{5-5}$$

Where, $r_{i,j}(BU_j)$ is the contribution of response to a detector at location i from the assembly at location j with a burnup of BU_j. $r_{i,j}(BU_j)$ is determined by Equation 5-6.

$$r_{i,j}(BU_j) = \sum_{g=1}^{G} \Psi^*_{i,j} S_{j,g}(BU_j) \tag{5-6}$$

Using error propagation, the uncertainty in this response due to uncertainty in the burnup at each location, BU_j, is calculated by Equation 5-7.

$$\sigma^2_{R,i} = \sum_{j=1}^{N} \left(\frac{\partial r_{i,j}}{\partial BU} \right)^2 \sigma^2_{BU,j} \tag{5-7}$$

The derivative above is approximated by Equation 5-8.

$$\frac{\partial r_{i,j}}{\partial BU} \cong \frac{r_{i,j}(BU_j + \Delta B) - r_{i,j}(BU_j)}{\Delta B} \tag{5-8}$$

Where ΔB is a small value (taken as $0.01 BU_j$)

5.3 Predicted Detector Response

We now examine the predicted detector response for a variety of scenarios. A script in MATLAB was created to perform the calculation (See Appendix E). The base case is a 6x8 array of NU assemblies at a burnup of 5000 MWd/MTU and cooling time of 30 years. The array layout showing detector measurement locations are shown in Figure 5-1. Response is predicted for every detector location in the pool.

From this sample assembly layout, we can predict the relative detector response at each (x, y) location in the pool. These results are calculated using both the previous methodology[1] and the methodology developed in this thesis. Figures 5-2 and 5-3 show the results for the previous and new methodologies, respectively.

These results differ by up to 25% due to the modeling of sub-critical multiplication and the extended FOV of the detector. If there were assemblies with different burnup, the discrepancy should be even higher since the new method makes no assumption of source linearity with burnup.

5.4 Modeling of Different Pool Configurations

In this section we examine several fuel pool configurations representing the diversion of spent fuel. First, however, a realistic baseline must be examined in which there is some uncertainty in the assembly burnup. To accomplish this, the previous model was adjusted to add a 5% error to each assembly burnup. This is compared to the model with zero error, to see what types of fluctuations would be present simply due to burnup uncertainty. Results are shown in Figure 5-4. All deviations were less than 5%.

A total of four possible fuel diversion scenarios were examined, as follows:

- Substitution of a single spent fuel assembly with a "dummy" assembly containing no nuclear material in location (4,3).
- Substitution of a single spent fuel assembly with a fresh fuel assembly at (4,3).
- Substitution of one spent fuel assembly with a dummy assembly at (4,3) and one adjacent to at (4,4) it with a high burnup (7000 MWd/MTU) assembly to mask it.
- Substitution of alternating spent fuel assemblies with dummies in a checkerboard pattern.

It is worth noting that for all of the spent fuel diversion scenarios that follow, the only "calibration" that is done is setting the measurement at detector position (2, 2) to equal 1. This means that all numbers are relative. This is more realistic because it would be very difficult to obtain true calibration values for the detector without independent confirmation of the calibration assemblies.

The first configuration examined is where one assembly is replaced with a dummy assembly containing no source. The predicted response is shown in Figure 5-5. The change is extremely obvious, with a ~25% deviation for any of the 4 measurement locations surrounding the dummy assembly. However, for a measurement taken

anywhere else (i.e., not directly adjacent to the missing assembly), the deviation is too small to be picked out from random fluctuations that would be expected due to uncertainties in assembly burnup.

A more difficult scenario would be if a spent assembly was replaced with a fresh one. Although there would be only a very small intrinsic neutron source in the fresh assembly, it would still contribute a source due to induced sub-critical multiplication. Deviation results for this scenario are shown in Figure 5-6. The deviation is only slightly smaller than for an inert dummy, and is still obvious with a 20-25% difference. Again, the deviation is only noticeable directly adjacent to the replaced assembly.

Another pool configuration would involve the replacement of one assembly with a fresh assembly and an adjacent one with a high burnup assembly (in this case 7000 MWd/MTU) to mask the lack of activity from the fresh fuel. This defect would not be visible to a detector in between the two modified assemblies, but it would show up at any location adjacent to only one of them. This is shown in Figure 5-7.

A more variant configuration, but potentially difficult to detect, would be a "checkerboard" pattern that would involve alternating fresh-fuel assemblies with high burnup assemblies such that the total source from the high burnup is the same. Without independent calibration, the assemblies could also be standard burnup, since all that will be seen are relative values. This scenario is shown in Figure 5-8. This shows very little deviation throughout except for the four corner locations where the deviation is large. This indicates that a corner location should always be tested.

5.5 Neutron to Gamma Response Ratio

Another method to determine the impact of configuration changes is to look at the ratio of neutron response to gamma response. This holds promise since the ratio of

neutron to gamma source varies with both cooling time and burnup. This should make it possible to identify assemblies whose burnup and cooling time do not match what should be there.

The hypothetical neutron to gamma response ratio was calculated for all of the scenarios outlined above. However, these results should be taken with caution because the gamma detector importance calculation assumed a uniformly sensitive detector, which is not realistic. Different conclusions may be reached for a "real" detector.

It is expected that the ratio of neutron to gamma signals will not vary much since changes in both signals will tend to cancel out. On the other hand, the ratio will also vary less due to the standard uncertainty in assembly burnup; hence, a smaller signal deviation is required to confirm a change. To help quantify this, a type of signal to noise ratio was used to compare the neutron results to the ratio results.

The signal (Equation 5-9) is taken as the average of the deviation in the "detectable" locations (i.e., the 4 possible locations around the defect).

$$m = \frac{1}{N_D} \sum_{i \in D} d_i \tag{5-9}$$

Where, D is the set of detector locations from which the change is visible (i.e., the four locations surrounding the dummy assembly) and N_D is the number of these locations.

The noise (Equation 5-10) is the standard deviation of the deviation in all of the remaining detector locations.

$$\sigma = \sqrt{\frac{1}{N - N_D - 1} \sum_{i \notin D} \left(d_i - \sum_{i \notin D} \frac{d_i}{N - N_D} \right)^2} \tag{5-10}$$

The signal to noise ratio was calculated for the four defect scenarios outlined above. Results are shown in Table 5-1. The result is that the neutron to gamma signal is at best as good as the neutron signal (Inert and inert + high burnup substitution) and at worst practically incapable of detecting a defect (fresh assembly and checkerboard substitution). However, for a detector system that has been independently calibrated, the checkerboard scenario would stick out to either the neutron or the neutron to gamma ratio for a detector positioned anywhere. If the substitution was made to use high burnup assemblies to make the neutron level indistinguishable, then the neutron to gamma ratio will be distinguishable and vice versa.

These results were obtained for NU assemblies at 5000 MWd/MTU and 30 years cooling time. For other assembly types, the neutron to gamma ratio might prove more capable of detecting changes. However, it alone can clearly not be used as the primary detection method.

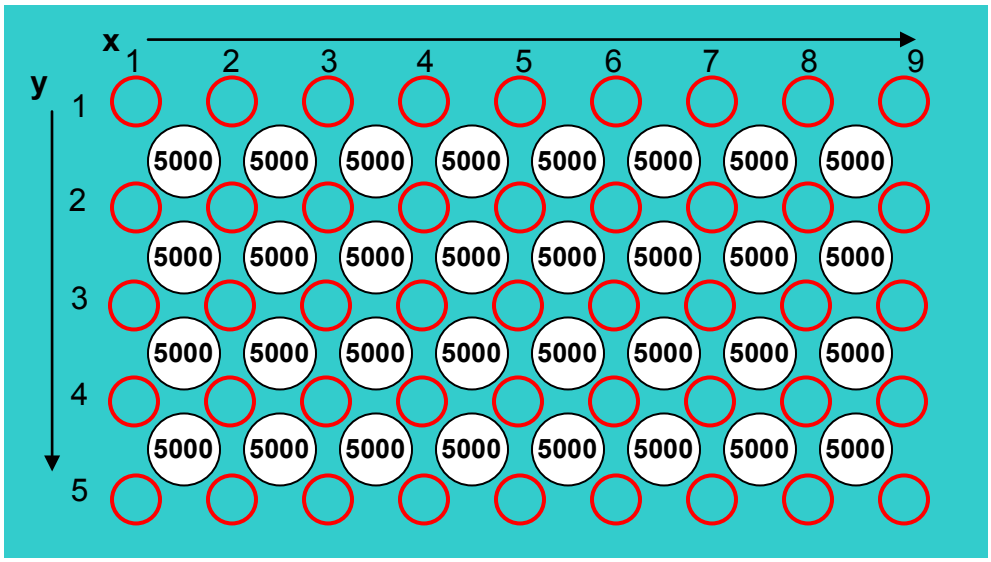

Figure 5-1. Layout of a sample spent fuel pool showing the assembly layout (white circles), the locations of (x, y) measurement positions (red circles) and total assembly burnups.

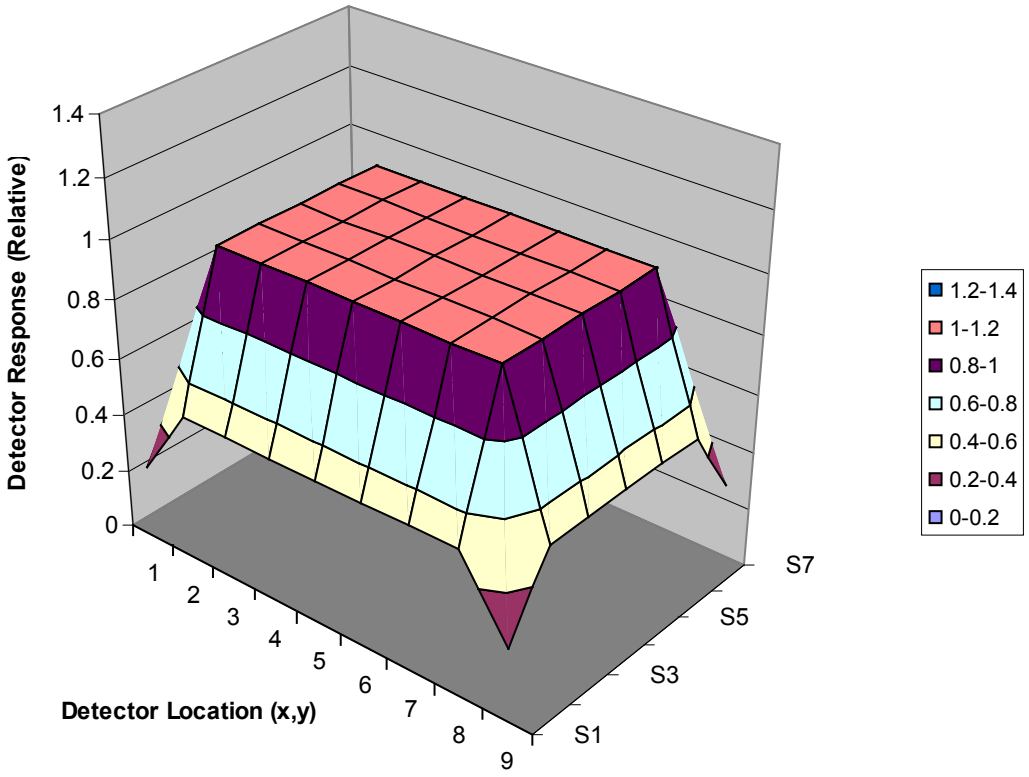

Figure 5-2. Predicted detector response for various detector positions using the sum-of-burnups method.

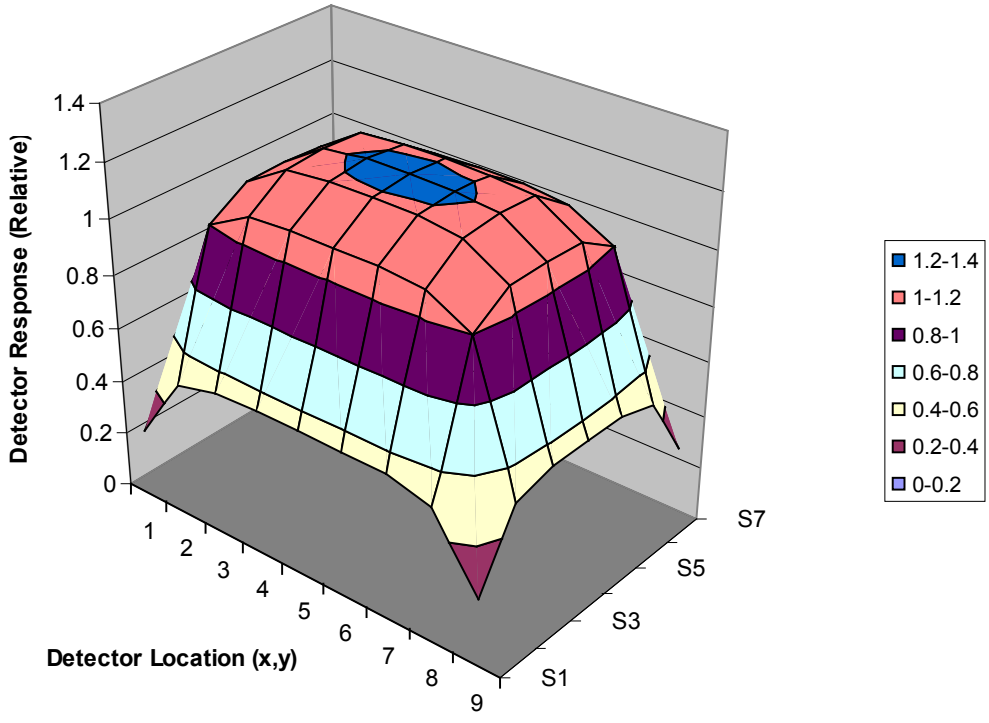

Figure 5-3. Predicted detector response for various detector positions using the new method incorporating detector importance and subcritical multiplication.

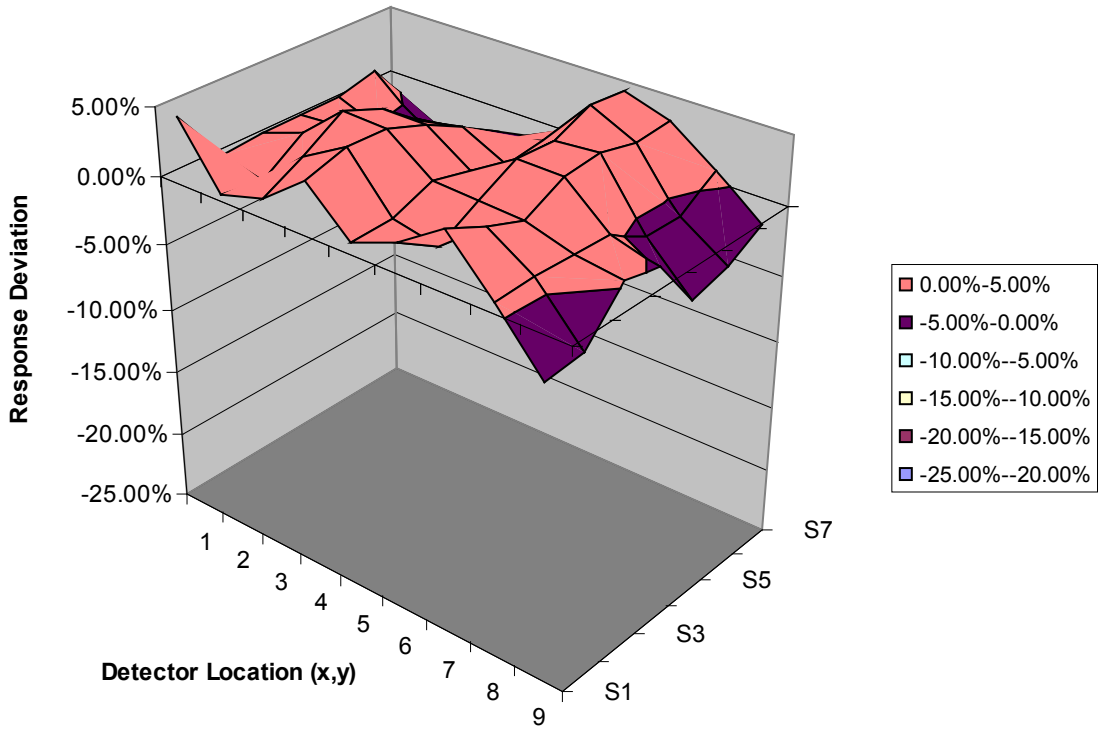

Figure 5-4. Predicted neutron detector response deviation for an array with 5% burnup variation compared with an array with no variation at 5000 MWd/MTU.

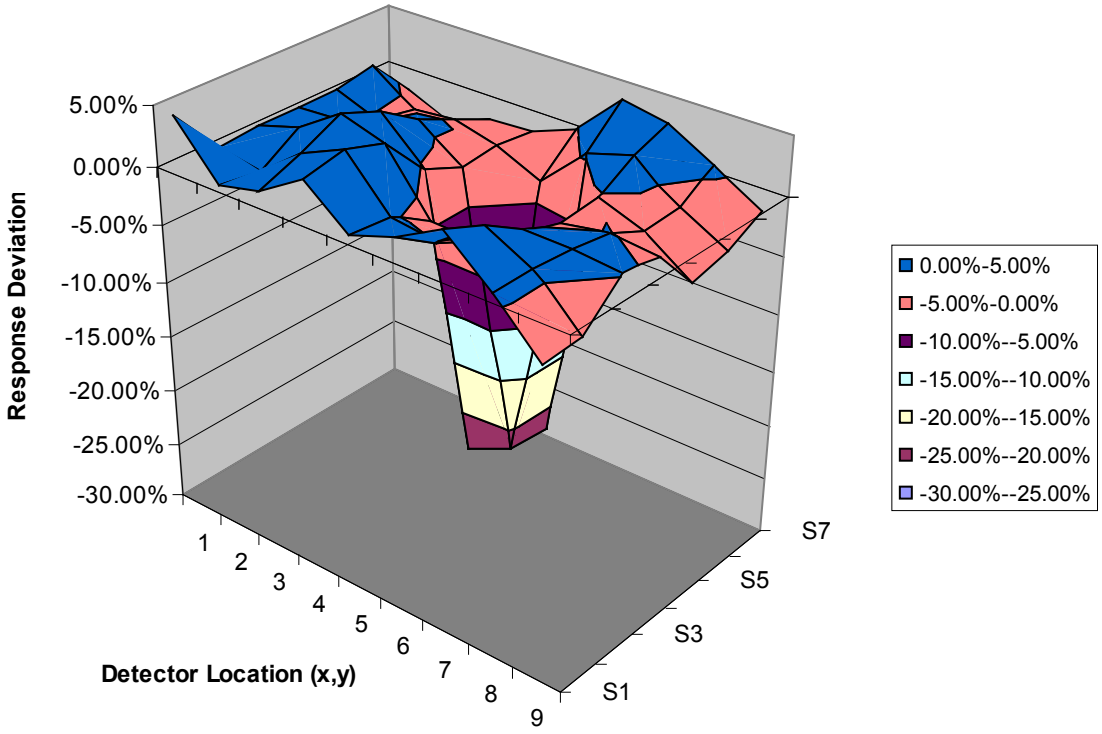

Figure 5-5. Predicted response deviation for substitution of one assembly with an inert dummy assembly.

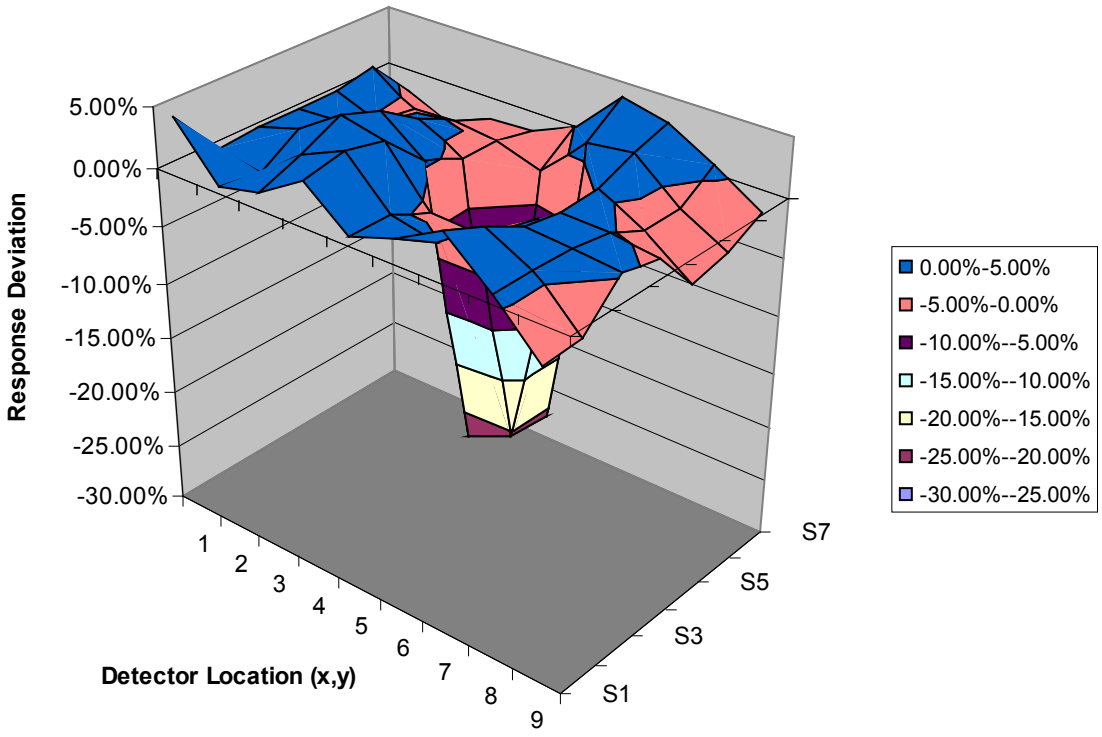

Figure 5-6. Predicted response deviation for substitution of one assembly with a fresh fuel dummy assembly.

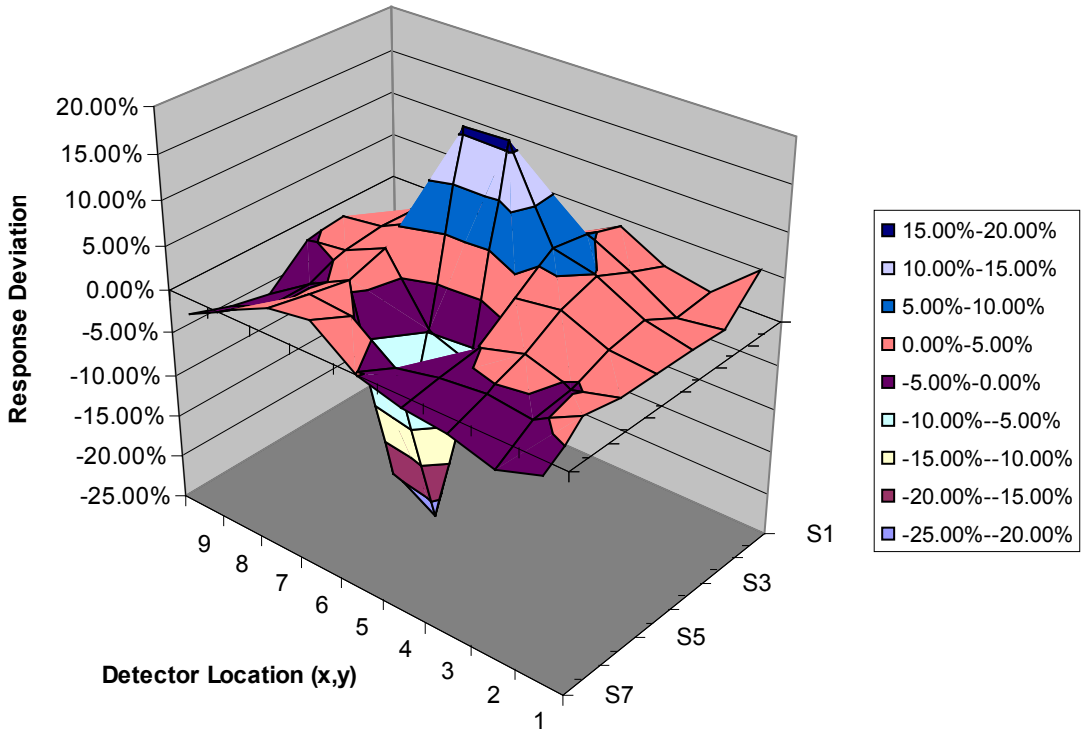

Figure 5-7. Predicted response deviation for substitution of a fresh fuel assembly and a high burnup assembly.

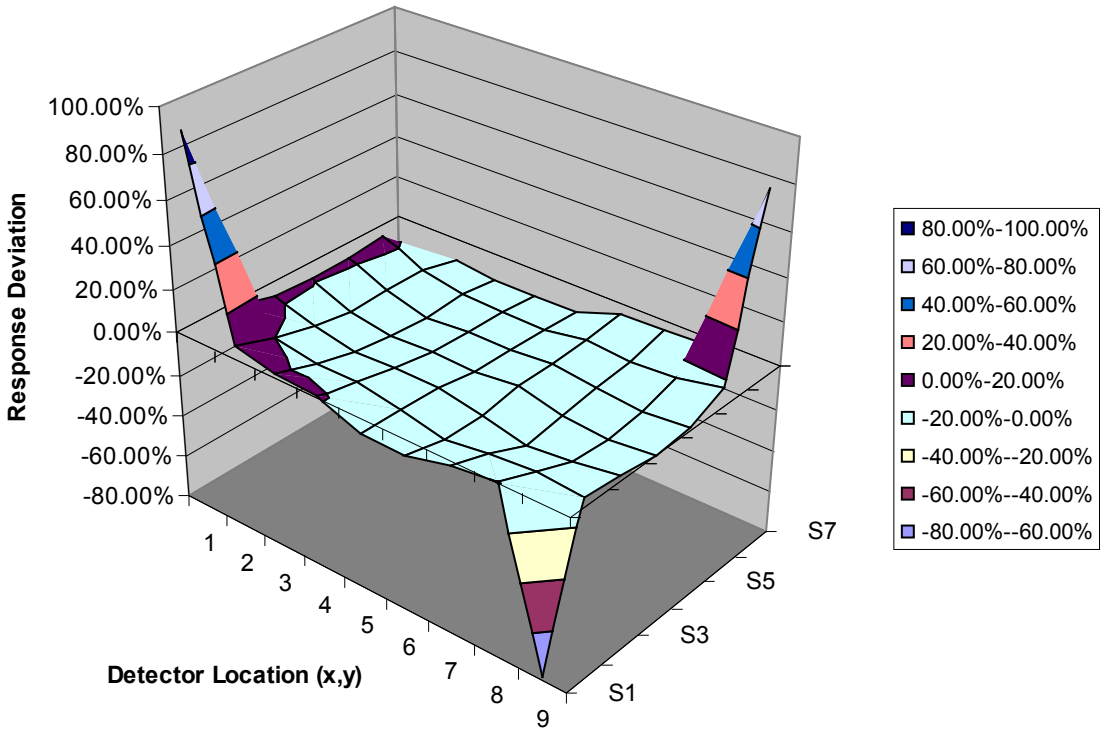

Figure 5-8. Predicted response deviation for a checkerboard substitution.

Table 5-1. Signal-to-Noise Ratios for Neutron signal and Neutron to Gamma Ratio for Various Substitution Scenarios

Substitution Scenario	Detector type	Average Signal (m)	Noise (σ)	SNR (m/σ)
Fresh Assembly	Neutron	-22.47%	2.13%	10.55
	N/G	- 2.10%	0.75%	2.80
Inert Assembly	Neutron	-23.57%	2.17%	10.85
	N/G	-3.54%	0.91%	3.88
Checkerboard	Neutron	+/- 81.36%	5.38%	15.13
	N/G	+ 10.84%	4.09%	2.65
Inert + High BU	Neutron	+/-20.96%	2.00%	10.46
	N/G	+9.60%	1.02%	9.42

CHAPTER 6
CONCLUSIONS

In this work, we demonstrated several improvements to previous methods to estimate detector response in a spent fuel pool (e.g., Atucha-I). The intrinsic source determination shows significant non-linear variation in the neutron source with both burnup and time. Sub-critical multiplication in the pool was shown to be very significant (multiplication factors up to 2.0) and a fast and accurate way of calculating this source distribution was developed using a simplified fission matrix method. This method can calculate the multiplication source in each assembly to within 5% for a wide variety of pool sizes and burnup histories. After a baseline Monte Carlo calculation time of ~10 hours, the method will work in ~1 sec for all subsequent calculations. The FOV of a thermal-neutron detector in the pool was determined using the importance methodology to be 87% within the 4 adjacent assemblies and 99% within the nearest 16. The FOV was fairly insensitive to detector location, with a difference of 5% for a location at the edge of the pool vs. the center. The FOV was also insensitive to burnup, with a less than 5% difference for an array of fresh assemblies compared with a group of assemblies at 11,000 MWd/MTU. For the cases studied, simulations of predicted detector response showed that the changes in the four conceived pool configurations were easily visible to a neutron detector placed adjacent to the changed assembly. For a checkerboard assembly substitution, a measurement at one of the corners was required to detect the change. In all scenarios, a deviation of at least 20% from the expected detector response was seen. To detect an assembly substitution, the detector response is compared to the predicted response. For the given burnup and burnup uncertainty, a deviation of 10-15% should warrant further inspection. The response of a

neutron detector to gamma detector was investigated, but proved to be less sensitive to changes than the neutron signal alone.

APPENDIX A
MCNP CRITICALITY INPUT DECK

```
c     Created on: Wednesday, May 21, 2008 at 14:43
c CELLS
c 0.838 mod density
c 0.979 mod (outside)
c 10.6 uo2 dens
c 6.5 zr dens
c 5.985 homogenized clad/gap zr dens
c OUTSIDE OF TUBE
    1     3   -0.979 104 -21 -22 31 -32 11 -12 imp:n=1  $mod outside tube
c COOLANT TUBE
    2     2    -6.5 101 -102 11 31 -42 imp:n=1     $inside tube
    3     0         102 -103 11 31 -42 imp:n=1          $annulus gas
    4     2    -6.5 103 -104 11 31 -42 imp:n=1     $outside tube
c OUTSIDE WORLD
   10     0         -11:42:21:22:-31:32 imp:n=0      $outside world
c UPPER MODERATOR
    5     3   -0.979 12 -42 104 -21 -22 31 -32 imp:n=1      $upper mod
    6     3   -0.838 12 -42 -101 -21 31 imp:n=1
c INNER MODERATOR
    7     3   -0.838 -101 11 -12 31 112 212 222 232 242 312 322
              332 342 352 362 412 422 432 442 452
              462 472 482 492 402 imp:n=1         $mod inside tube
c R0
   11     1   -10.6 -111 11 -12 31 imp:n=1         $pin 1
   12     2    -5.985 111 -112 11 -12 31 imp:n=1
c R1
  111     1   -10.6 -211 11 -12 31 imp:n=1
  112     2    -5.985 -212 211 11 -12 31 imp:n=1
  121     1   -10.6 -221 11 -12 imp:n=1
  122     2    -5.985 -222 221 11 -12 imp:n=1
  131     1   -10.6 -231 11 -12 imp:n=1
  132     2    -5.985 -232 231 11 -12 imp:n=1
  141     1   -10.6 -241 11 -12 31 imp:n=1
  142     2    -5.985 -242 241 11 -12 31 imp:n=1
c R2
  211     1   -10.6 -311 11 -12 imp:n=1
  212     2    -5.985 -312 311 11 -12 imp:n=1
  221     1   -10.6 -321 11 -12 imp:n=1
  222     2    -5.985 -322 321 11 -12 imp:n=1
  231     1   -10.6 -331 11 -12 imp:n=1
  232     2    -5.985 -332 331 11 -12 imp:n=1
  241     1   -10.6 -341 11 -12 imp:n=1
  242     2    -5.985 -342 341 11 -12 imp:n=1
  251     1   -10.6 -351 11 -12 imp:n=1
  252     2    -5.985 -352 351 11 -12 imp:n=1
  261     1   -10.6 -361 11 -12 imp:n=1
  262     2    -5.985 -362 361 11 -12 imp:n=1
c R3
  311     1   -10.6 -411 11 -12 imp:n=1
  312     2    -5.985 -412 411 11 -12 imp:n=1
  321     1   -10.6 -421 11 -12 imp:n=1
  322     2    -5.985 -422 421 11 -12 imp:n=1
  331     1   -10.6 -431 11 -12 imp:n=1
```

```
  332     2    -5.985 -432 431 11 -12 imp:n=1
  341     1   -10.6 -441 11 -12 imp:n=1
  342     2    -5.985 -442 441 11 -12 imp:n=1
  351     1   -10.6 -451 11 -12 imp:n=1
  352     2    -5.985 -452 451 11 -12 imp:n=1
  361     1   -10.6 -461 11 -12 imp:n=1
  362     2    -5.985 -462 461 11 -12 imp:n=1
  371     1   -10.6 -471 11 -12 imp:n=1
  372     2    -5.985 -472 471 11 -12 imp:n=1
  381     1   -10.6 -481 11 -12 imp:n=1
  382     2    -5.985 -482 481 11 -12 imp:n=1
  391     1   -10.6 -491 11 -12 31 imp:n=1
  392     2    -5.985 -492 491 11 -12 31 imp:n=1
c STRUCT PIN
c 3101     1   -10.6 -401 11 -12 31 imp:n=1
 3102     2    -6.5 -402 11 -12 31 imp:n=1

c SURFACES
  *11        pz 0
   12        pz 265
  *21        p 1.0 0.57735027 0 15.703927 $ pitch/2 / cos30
  *22        p -1.0 0.57735027 0 15.703927
  *31        py 0
  *32        py 13.6
c   61       p 1.0 0.57735027 0 0
c   62       p -1.0 0.57735027 0 0
c   41        pz -100
   42        pz 315
   51       pz 26.5
   52       pz 53
   53       pz 79.5
   54       pz 106
   55       pz 132.5
   56       pz 159
   57       pz 185.5
   58       pz 212
   59       pz 238.5
  101       c/z 0 0 5.410
  102       c/z 0 0 5.582
  103       c/z 0 0 5.750
  104       c/z 0 0 5.790
c      r0
  111       c/z 0 0 0.535
  112       c/z 0 0 0.595
c      r1
  221       c/z 0.811 1.4047 0.535
  222       c/z 0.811 1.4047 0.595
  211       c/z 1.622 0 0.535
  212       c/z 1.622 0 0.595
  231       c/z -0.811 1.4047 0.535
  232       c/z -0.811 1.4047 0.595
  241       c/z -1.622 0 0.535
  242       c/z -1.622 0 0.595
c      r2
  311       c/z 2.9654 0.7946 0.535
  312       c/z 2.9654 0.7946 0.595
  331       c/z 0.7946 2.9654 0.535
```

```
  332       c/z 0.7946 2.9654 0.595
  321       c/z 2.1708 2.1708 0.535
  322       c/z 2.1708 2.1708 0.595
  361       c/z -2.9654 0.7946 0.535
  362       c/z -2.9654 0.7946 0.595
  341       c/z -0.7946 2.9654 0.535
  342       c/z -0.7946 2.9654 0.595
  351       c/z -2.1708 2.1708 0.535
  352       c/z -2.1708 2.1708 0.595
c      r3
c  401       c/z 4.553 0 0.535
  402       c/z 4.553 0 0.595
  411       c/z 4.2784 1.5572 0.535
  412       c/z 4.2784 1.5572 0.595
  431       c/z 2.2765 3.943 0.535
  432       c/z 2.2765 3.943 0.595
  421       c/z 3.4878 2.9266 0.535
  422       c/z 3.4878 2.9266 0.595
  441       c/z 0.7906 4.4838 0.535
  442       c/z 0.7906 4.4838 0.595
  491       c/z -4.553 0 0.535
  492       c/z -4.553 0 0.595
  481       c/z -4.2784 1.5572 0.535
  482       c/z -4.2784 1.5572 0.595
  461       c/z -2.2765 3.943 0.535
  462       c/z -2.2765 3.943 0.595
  471       c/z -3.4878 2.9266 0.535
  472       c/z -3.4878 2.9266 0.595
  451       c/z -0.7906 4.4838 0.535
  452       c/z -0.7906 4.4838 0.595
c

c DATA
c f7:n 521 522 523 524 525 526 527 528 529 520
c     (521 522 523 524 525 526 527 528 529 520)
c     41 51 61 81 91 101 111
E0 1.75e-7 1.0e-6 1.0e-4 1.0e-2 1.0e-1 1 20
f4:n  11 111 121 131 141 211 221 231 241 251 261
      311 321 331 341 351 361 371 381 391
fs4  -51 -52 -53 -54 -55 -56 -57 -58 -59 T
SD4   (1.2629e+02 1.2629e+02 1.2629e+02 1.2629e+02 1.2629e+02
      1.2629e+02 1.2629e+02 1.2629e+02 1.2629e+02 1.2629e+02
      1.2629e+03)
f7:n  11 111 121 131 141 211 221 231 241 251 261
      311 321 331 341 351 361 371 381 391
fs7  -51 -52 -53 -54 -55 -56 -57 -58 -59 T
SD7   (1.2629e+02 1.2629e+02 1.2629e+02 1.2629e+02 1.2629e+02
      1.2629e+02 1.2629e+02 1.2629e+02 1.2629e+02 1.2629e+02
      1.2629e+03)
fmesh14:n GEOM=xyz ORIGIN -16.0 0 0
        IMESH=16.0 IINTS=20
        JMESH=16.0 JINTS=10
        KMESH=265.0 KINTS=5
        EMESH=1.75e-7 1.0e-6 1.0e-4 1.0e-2
        1.0e-1 1 20 EINTS= 1 1 1 1 1 1 1
mode n
kcode 100 1 10 100
```

```
ksrc 0 .1 25
     0 .1 50
     0 .1 75
     0 .1 100
     0 .1 125
     0 .1 150
     0 .1 175
     0 .1 200
     0 .1 225
     0 .1 250
c    fuel
m1    92235.60c           0.0085  $.85% enriched U
      92238.60c           0.9915
      8016.60c            2
m2    40000.60c                1  $zirc
m3    1002.60c                 2  $D2O
      8016.60c                 1
mt3   hwtr.62t  $S(A,B) endf6.3 600K
```

APPENDIX B
MCNP FISSION MATRIX INPUT DECK

```
c     Created on: Wednesday, Sept 26, 2008
c CELLS
c r1 -4.89
c r2 -5.07
c r3 -4.55
c
c ******************* LATTICE ELEMENT 7 **********************
c
c Ring one stuff
201   21 -4.89 -9 -10  imp:n=1   u=7 vol=1374.5895 $first axial zone (center)
for ring 1
c
c Ring two stuff
209   22 -5.07 -9 10 -11 imp:n=1 u=7 vol=2253.7578 $second axial zone
(center) for ring 1
c
c Ring three stuff
2017  23 -4.55 -9 11 -12 imp:n=1 u=7 vol=3681.5543 $third axial zone (center)
for ring 1
c
c Water Above
2029  4 -1.0  9 -12 imp:n=1 u=7
c
2025  4 -1.0  12 imp:n=1 u=7 vol=1 $water region outside rings
c
c water region
26  4 -1.0     -101 100 -103 102 imp:n=1 u=1 lat=1 fill= -6:6 -4:5 0:0
$water region in assy
                     1 1 1 1 1 1 1 1 1 1 1 1 1
                     1 1 1 1 1 1 1 1 1 1 1 1 1
                     1 1 7 7 7 7 7 7 7 7 7 1 1
                     1 1 7 7 7 7 7 7 7 7 7 1 1
                     1 1 7 7 7 7 7 7 7 7 7 1 1
                     1 1 7 7 7 7 7 7 7 7 7 1 1
                     1 1 7 7 7 7 7 7 7 7 7 1 1
                     1 1 7 7 7 7 7 7 7 7 7 1 1
                     1 1 1 1 1 1 1 1 1 1 1 1 1
                     1 1 1 1 1 1 1 1 1 1 1 1 1
c lattice
27     0         204 -205 206 -207 1 -13 imp:n=1  fill=1
c outside world
28 0          -204:205:-206:207:-1:13 imp:n=0  $outside world

c
c Surfaces
c z surfaces
*1   pz 0       $midplane of assy, only model to half
2   pz 79.5    $top of zone 1 source
3   pz 106   $top of zone 2 source
4   pz 132.5   $top of zone 3 source
5   pz 159   $top of zone 4 source
6   pz 185.5   $top of zone 5 source
7   pz 212   $top of zone 6 source
```

```
8   pz 238.5   $top of zone 7 source
9   pz 265     $top of fuel (zone 8 source)
13  pz 315     $top of shield water
c
c cylinders for source regions radially
10  cz  2.346   $Inner ring radius
11  cz  3.8115  $Middle ring radius
12  cz  5.41    $Outer ring radius
c
c outer x/y boundary
100 px -7.25   $left boundary of single assy lattice element
101 px 7.25    $right boundary of single assy lattice element
102 py -7.5   $front boundary of single assy lattice element
103 py 7.5    $back boundary of single assy lattice element
c
c 4X4 assy lattice boundary
204 px -94.25
205 px 94.25
206 py -67.5
207 py 82.5
c
c Detector
300 c/z 7.25 7.5 1.27
301 c/z 7.25 7.5 3.0

c DATA CARDS
c
mode n
c
c Source
sdef  erg d1 pos 0 0 0 rad d3 ext d4 axs 0 0 1
si1   H 1.00E-11 1.00E-07 4.14E-07 8.76E-07 1.86E-06 5.04E-06 1.07E-05
        3.73E-05 1.01E-04 2.14E-04 4.54E-04 1.58E-03 3.35E-03 7.10E-03
        1.50E-02 2.19E-02 2.42E-02 2.61E-02 3.18E-02 4.09E-02 6.74E-02
        1.11E-01 1.83E-01 2.97E-01 3.69E-01 4.98E-01 6.08E-01 7.43E-01
        8.21E-01 1.00E+00 1.35E+00 1.65E+00 1.92E+00 2.23E+00 2.35E+00
        2.37E+00 2.47E+00 2.73E+00 3.01E+00 3.68E+00 4.97E+00 6.07E+00
        7.41E+00 8.61E+00 1.00E+01 1.22E+01 1.42E+01 1.98E+01
sp1     0 1.05148E-11 9.19638E-11 2.06605E-10 6.06981E-10 3.00603E-09
        7.86288E-09 6.3109E-08 2.81517E-07 7.41587E-07 2.26519E-06
        1.84003E-05 4.5103E-05 0.000139905 0.000431693 0.000484179
        0.000181718 0.000155726 0.000509543 0.000891512 0.003136615
        0.006506781 0.013400301 0.02553993 0.017880462 0.034781517
        0.031265696 0.03915118 0.023016072 0.053641386 0.102209945
        0.084957308 0.074058262 0.084329483 0.030361627 0.005123054
        0.025966851 0.062757408 0.060497238 0.098543446 0.076770467
        0.024726268 0.012127072
        0.003965344 0.001635359 0.000629332 9.14616E-05 1.96359E-05
si3   S 5 6 7
sp3   1.404 2.779 6.442
si4   0 265
si5   0 2.346
sp5   -21 1
si6   2.346 3.8115
sp6   -21 1
si7   3.8115 5.41
sp7   -21 1
```

```
nonu
nps 500000
c
c Tally Cards
f4:n   (201<u=7)
sd4    1 53r
fm4    7.53820E-02 21 -6 -7
f14:n  (209<u=7)
sd14   1 53r
fm14   7.47385E-02 22 -6 -7
f24:n  (2017<u=7)
sd24   1 53r
fm24   7.55275E-02 23 -6 -7
c
c Material cards
c
c    fuel ring 1
c
c 94% U detector
m1    92235.66c -0.94
      92238.66c -0.06
c Al casing
m2    13027.66c 1
c Poly
m3    1001.60c  2
      6000.60c  1
mt3   poly.60t
m5    40000.60c               1  $zirc
m4    1001.60c                2  $H2O
      8016.60c                1
mt4   lwtr.60t  $S(A,B)
c
m21           95241.66c        1.07E-04
        64155.66c        1.80E-06
        60143.50c        3.61E-04
        60145.50c        2.85E-04
        94239.66c        2.38E-03
        94240.66c        7.29E-04
        94241.66c        3.33E-05
        45103.66c        3.41E-04
        62149.66c        2.04E-06
        62151.50c        3.90E-06
        43099.66c        5.03E-04
        92235.66c        2.96E-03
        92236.66c        9.30E-04
        92238.66c        9.91E-01
        54131.66c        2.42E-04
      8016.60c            4.216
      1001.60c            4.31
      40000.60c           1.20
mt21   lwtr.60t  $S(A,B) 294k
c    fuel ring 2
m22     95241.66c        1.21E-04
        64155.66c        1.97E-06
        60143.50c        3.82E-04
        60145.50c        3.06E-04
        94239.66c        2.45E-03
```

```
        94240.66c        8.05E-04
        94241.66c        3.77E-05
        45103.66c        3.71E-04
        62149.66c        2.16E-06
        62151.50c        4.02E-06
        43099.66c        5.43E-04
        92235.66c        2.75E-03
        92236.66c        9.74E-04
        92238.66c        9.91E-01
        54131.66c        2.61E-04
      8016.60c            3.99
      1001.60c            3.97
      40000.60c           1.20
mt22   lwtr.60t  $S(A,B) 294k
c    fuel ring 3
m23           95241.66c        1.48E-04
        64155.66c        2.31E-06
        60143.50c        4.19E-04
        60145.50c        3.45E-04
        94239.66c        2.55E-03
        94240.66c        9.43E-04
        94241.66c        4.59E-05
        45103.66c        4.27E-04
        62149.66c        2.39E-06
        62151.50c        4.23E-06
        43099.66c        6.17E-04
        92235.66c        2.41E-03
        92236.66c        1.05E-03
        92238.66c        9.91E-01
        54131.66c        2.96E-04
      8016.60c            4.54
      1001.60c            5.08
      40000.60c           1.27
mt23   lwtr.60t  $S(A,B) 294k
```

APPENDIX C
FISSION MATRIX SCRIPT

```
function out1=fissionMatrix(ftype,nx,ny,S,xbu,xt)
%fmatrix(ftype,nx,ny,Sint,xbu,xt)
%ftype      type of fuel (1 = NU, 2 = SEU *not implemented*)
%nx   number of assemblies in x direction
%ny   number of assemblies in y direction
%S    intrinsic source of each assembly size=(x,y,G)
%xbu  burnup of each assembly (x,y)
%     0=fresh -1=inert
%xt   cooling time of each assembly (x,y)

ix=0;
iy=0;
fmult=ones(nx,ny);
F=ones(nx,ny);
Fold=ones(nx,ny);

if ftype==2
%SEU fuel
    M(1,1)=0.21715;    M(1,2)=0.05778;    M(2,1)=0.05778;
    M(2,2)=0.01894;    M(3,1)=0.00369;    M(1,3)=0.00369;
    M(3,2)=0.00188;    M(2,3)=0.00188;    M2(1,1)=0.21926;
    M2(1,2)=0.05800;   M2(2,1)=0.05800;   M2(2,2)=0.01889;
    M2(3,1)=0.00370;   M2(1,3)=0.00370;   M2(3,2)=0.00186;
    M2(2,3)=0.00186;   M3(1,1)=0.22141;   M3(1,2)=0.05811;
    M3(2,1)=0.05811;   M3(2,2)=0.01881;   M3(3,1)=0.00369;
    M3(1,3)=0.00369;   M3(3,2)=0.00190;   M3(2,3)=0.00190;
else
%NU fuel
%FISSION MATRIX COEFFICIENTS
    Mt(:,:,1,1)=[2.13E-01     4.98E-02    2.70E-03;
            4.56E-02    1.38E-02    1.22E-03;
            2.18E-03    1.11E-03    0]';
    Mt(:,:,1,2)=[2.14E-01     4.98E-02    2.69E-03;
            4.57E-02    1.37E-02    1.22E-03;
            2.17E-03    1.08E-03    0]';
    Mt(:,:,1,3)=[2.15E-01     5.00E-02    2.66E-03;
            4.58E-02    1.38E-02    1.22E-03;
            2.17E-03    1.08E-03    0]';
      Mt(:,:,2,1)=[     2.18E-01    5.14E-02    2.78E-03;
                        4.71E-02    1.43E-02    1.26E-03;
                        2.25E-03    1.14E-03    0]';
        Mt(:,:,3,1)=[   2.05E-01    4.77E-02    2.57E-03;
                  4.37E-02    1.33E-02    1.17E-03;
                  2.09E-03    1.05E-03    0.00E+00]';
        Mt(:,:,4,1)=[   1.93E-01    4.45E-02    2.41E-03;
                  4.08E-02    1.24E-02    1.09E-03;
                  1.95E-03    9.83E-04    0.00E+00]';
      Mt(:,:,2,2)=[     2.20E-01    5.16E-02    2.78E-03;
                        4.74E-02    1.42E-02    1.26E-03;
                        2.25E-03    1.13E-03    0]';
        Mt(:,:,3,2)=[2.06E-01 4.79E-02    2.57E-03;
                     4.40E-02  1.32E-02    1.17E-03;
                     2.07E-03  1.04E-03    0]';
```

```
        Mt(:,:,4,2)=[1.94E-01 4.45E-02    2.39E-03;
                     4.09E-02  1.22E-02    1.09E-03;
                     1.91E-03  9.69E-04    0]';
      Mt(:,:,2,3)=[2.21E-01   5.18E-02    2.75E-03;
                     4.75E-02  1.42E-02    1.27E-03;
                     2.26E-03  1.13E-03    0]';
        Mt(:,:,3,3)=[2.07E-01 4.79E-02    2.55E-03;
                     4.41E-02  1.32E-02    1.17E-03;
                     2.07E-03  1.02E-03    0]';
        Mt(:,:,4,3)=[1.95E-01 4.45E-02    2.37E-03
                     4.09E-02  1.22E-02    1.10E-03
                     1.93E-03  9.56E-04    0]';

    %COOLING TIME AND BURNUP FOR THESE COEFFICIENTS
    t=[30 1 1 30];
    bu=[5000 5000 8000 8000];


    for ix=1:nx
    %FOR EACH ASSEMBLY
        for iy=1:ny
            if ((ix==1) || (ix==nx) || (iy==1) || (iy==ny))
            %EDGE assembly
                    ii=2;
                    if ((ix==1) || (ix==nx)) && ((iy==1) || (iy==ny))
                    %CORNER assembly
                        ii=3;
                    end
            else
            %INTERIOR assembly
                ii=1;
            end

            if xbu(ix,iy)<0
            %INERT assembly
                fmult(ix,iy)=0;
            end
            if xbu(ix,iy)<4000
            %FRESH assembly
                xbu(ix,iy)=5000;
            end

            %Interpolate FM coefficient in cooling time and burnup
            bM1=Mt(:,:,2,ii)+(Mt(:,:,3,ii)-Mt(:,:,2,ii))/(bu(3)-
bu(2))*(xbu(ix,iy)-bu(2));
            bM2=Mt(:,:,1,ii)+(Mt(:,:,4,ii)-Mt(:,:,1,ii))/(bu(4)-
bu(1))*(xbu(ix,iy)-bu(1));
            tM1=bM1+(bM2-bM1)/(t(1)-t(2))*(xt(ix,iy)-t(2));
            M(ix,iy,:,:)=tM1*fmult(ix,iy);
        end
    end
end

%make sure FM coefficient array is big enough
M=padarray(M,[0 0 nx ny],0,'post');
maxerr=1;
newerr=0;
```

```
iter=0;

%Gauss-Siedel Iteration solve for F
while (maxerr>0.000001)
    iter=iter+1;
    maxerr=0;
    for ix=1:nx
        for iy=1:ny
            Fold(ix,iy)=F(ix,iy);
            F(ix,iy)=0;
            for iix=1:nx
                for iiy=1:ny
                    F(ix,iy)=F(ix,iy)+M(ix,iy,abs(iix-ix)+1,abs(iiy-
iy)+1)*(Fold(iix,iiy)...
                        +S(iix,iiy));
                end
            end
            newerr=abs((F(ix,iy)-Fold(ix,iy))/(Fold(ix,iy)+1e-10));
            if newerr>maxerr
                maxerr=newerr;
            end
        end
    end

    if iter>2000
        maxerr=0;
    end
end

Fp=F/sum(sum(S));
mult=sum(sum(Fp));

out1=F;
end
```

APPENDIX D
PENTRAN INPUT

```
   PARAMETERS FOR MEMORY ALLOCATION using F90:
    maxmem,    maxpcs,    maxgcm,    maxxsg
       2000         2          4         47
    maxcmc,    maxcrs,   maxmmc,   maxmed,   maxfmc,   maxfin
         4          2      2500       100      2500       100
    maxgrp,    maxglc,   maxswp,   maxqdm,   maxmat,   maxleg
        47         47         4          3         14          3
    maxsrc,    maxslc,   maxcmr,   maxlin,   maxarr,   nctlim
         1          1          4       228    117500       183
/-----------------Start Problem Deck---------------
2dNU55                                                                  loglevel
2
generated by PENMSHXP version 1.7 (June 2008)
Total Number of Fine Meshes:  10000
Total Number of Coarse Meshes:  4
Number of zlevs:  1
Number of coarse mesh per z lev: 4
6
7
8
9
10
/
/-------------BLOCK I (GENERAL PROBLEM info.)-----------
/
ngeom=3d
modadj=1
ngroup=47    1
isn=4
nmatl=14
ixcrs=2
jycrs=2
kzcrs=1
lodbal=0
timcut=0.
tolmgd=-0.200
decmpv=-4 -1 -1  T
/
/------------------BLOCK II(geometry)-----------------
/
/ x coarse-mesh position
/
xmesh= 0.0000E+00  1.4500E+01  2.9000E+01
/
/ x fine mesh distribution for zlev=  1
/
ixfine=50 50
       50 50
/
/ x medium mesh distribution for zlev=  1
/
ixmed=50 50
      50 50
```

```
/
/ y coarse-mesh position
/
ymesh= 0.0000E+00  1.5000E+01  3.0000E+01
/
/ y fine mesh distribution for zlev=  1
/
jyfine=50 50
       50 50
/
/ y medium mesh distribution for zlev=  1
/
jymed=50 50
      50 50
/
/ z coarse-mesh position
/
zmesh= 0.0000E+00  1.2700E+01
/
/ z fine mesh distribution for zlev=  1
/
kzfine=1 1
       1 1
/
/ z medium mesh distribution for zlev=  1
/
kzmed=1 1
      1 1
/
/  material distribution for zlev=  1
/
    nmattp=1
4R6 6R5 40R4 2Q50 2R6 8R5 40R4 9R5 41R4 1Q50 8R5 42R4 7R5 43R4 5R5 15R4 10R11
20R4 3R5 14R4 16R11 33R4 18R11 30R4 22R11 27R4 24R11 25R4 10R11 6R10 10R11
23R4 8R11 12R10 8R11 21R4 8R11 14R10 8R11 20R4 6R11 18R10 6R11 19R4 7R11
18R10
7R11 18R4 6R11 7R10 6R9 7R10 6R11 17R4 6R11 7R10 8R9 7R10 6R11 16R4 6R11 6R10
10R9 6R10 6R11 16R4 5R11 6R10 12R9 6R10 5R11 15R4 6R11 5R10 14R9 5R10 6R11
5Q50 15R4 5R11 6R10 12R9 6R10 5R11 16R4 6R11 6R10 10R9 6R10 6R11 16R4 6R11
7R10 8R9 7R10 6R11 17R4 6R11 7R10 6R9 7R10 6R11 18R4 7R11 18R10 7R11 19R4
6R11
18R10 6R11 20R4 8R11 14R10 8R11 21R4 8R11 12R10 8R11 23R4 10R11 6R10 10R11
25R4 24R11 27R4 22R11 30R4 18R11 33R4 16R11 37R4 10R11 420R4
    nmattp=2
420R4 10R11 37R4 16R11 33R4 18R11 30R4 22R11 27R4 24R11 25R4 10R11 6R10 10R11
23R4 8R11 12R10 8R11 21R4 8R11 14R10 8R11 20R4 6R11 18R10 6R11 19R4 7R11
18R10
7R11 18R4 6R11 7R10 6R9 7R10 6R11 17R4 6R11 7R10 8R9 7R10 6R11 16R4 6R11 6R10
10R9 6R10 6R11 16R4 5R11 6R10 12R9 6R10 5R11 15R4 6R11 5R10 14R9 5R10 6R11
5Q50 15R4 5R11 6R10 12R9 6R10 5R11 16R4 6R11 6R10 10R9 6R10 6R11 16R4 6R11
7R10 8R9 7R10 6R11 17R4 6R11 7R10 6R9 7R10 6R11 18R4 7R11 18R10 7R11 19R4
6R11
18R10 6R11 20R4 8R11 14R10 8R11 21R4 8R11 12R10 8R11 23R4 10R11 6R10 10R11
25R4 24R11 27R4 22R11 30R4 18R11 33R4 16R11 37R4 10R11 420R4
    nmattp=3
322R4 6R11 40R4 14R11 34R4 18R11 30R4 22R11 27R4 24R11 25R4 26R11 23R4 9R11
```

```
10R10 9R11 21R4 8R11 14R10 8R11 20R4 7R11 16R10 7R11 19R4 7R11 18R10 7R11
18R4
6R11 9R10 2R9 9R10 6R11 17R4 6R11 7R10 8R9 7R10 6R11 16R4 6R11 6R10 10R9 6R10
6R11 16R4 5R11 6R10 12R9 6R10 5R11 15R4 6R11 5R10 14R9 5R10 6R11 5Q50 15R4
5R11 6R10 12R9 6R10 5R11 16R4 6R11 5R10 12R9 5R10 6R11 16R4 6R11 6R10 10R9
6R10 6R11 16R4 7R11 7R10 6R9 7R10 7R11 17R4 6R11 20R10 6R11 18R4 7R11 18R10
7R11 19R4 7R11 16R10 7R11 21R4 8R11 12R10 8R11 23R4 9R11 8R10 9R11 24R4 26R11
26R4 22R11 29R4 20R11 32R4 16R11 36R4 12R11 519R4
    nmattp=4
322R4 6R11 40R4 14R11 34R4 18R11 30R4 22R11 27R4 24R11 25R4 26R11 23R4 9R11
10R10 9R11 21R4 8R11 14R10 8R11 20R4 7R11 16R10 7R11 19R4 7R11 18R10 7R11
18R4
6R11 9R10 2R9 9R10 6R11 17R4 6R11 7R10 8R9 7R10 6R11 16R4 6R11 6R10 10R9 6R10
6R11 16R4 5R11 6R10 12R9 6R10 5R11 15R4 6R11 5R10 14R9 5R10 6R11 5Q50 15R4
5R11 6R10 12R9 6R10 5R11 16R4 6R11 5R10 12R9 5R10 6R11 16R4 6R11 6R10 10R9
6R10 6R11 16R4 7R11 7R10 6R9 7R10 7R11 17R4 6R11 20R10 6R11 18R4 7R11 18R10
7R11 19R4 7R11 16R10 7R11 21R4 8R11 12R10 8R11 23R4 9R11 8R10 9R11 24R4 26R11
26R4 22R11 29R4 20R11 32R4 16R11 36R4 12R11 519R4
flxini=4R0.000
mathmg=4R0    T
/
/ ------------- BLOCK III (CROSS SECTIONS) -----------
/
lib=file:nuall.xs
legord=1  legoxs=3
nxtyp=1
ihm=50
iht=3  ihs=4
ihng=0
chig=1.0000E+00 46R0.0000E+00 13Q47
nxcmnt=2    T
/
/------------- BLOCK IV (CONTROL OPTIONS) --------------
/
ncoupl=1
nprtyp=1
nrdblk=0
tolin=2.00E-03
tolout=1.00E-05
dtwmxw=0.95
maxitr=1000    10
methit=1
/
/  Starting or selected differencing scheme,for each coarse-mesh, for z-
level=   1
/
ndmeth=2 2
       2 2
nzonrb=4  0.999  0
methac=1      T
/------------------BLOCK V(source)------------------
/
nsdef=0
nscmsh=1
sref=3R0.000
serg=4.43E-01
1.72E-01 5.83E-02 3.97E-02 2.17E-02 5.94E-02 6.42E-02 3.69E-02
```

```
2.43E-02 1.71E-02 1.02E-02 5.86E-03 3.96E-03 2.88E-03 2.32E-03 2.20E-03
2.10E-03 2.04E-03 1.89E-03 1.72E-03 1.50E-03 1.30E-03 1.13E-03 1.04E-03
9.83E-04 9.27E-04 9.05E-04 8.92E-04 9.08E-04 9.39E-04 9.51E-04 9.61E-04
9.59E-04 9.49E-04 9.44E-04 9.40E-04 9.27E-04 9.02E-04 8.65E-04 8.11E-04
7.66E-04 9.99E-04 1.26E-03 1.28E-03 1.25E-03 1.38E-03 1.50E-03
smag=1
spacpf=1   -1        2500
4R7.14286E-02 46R0.00000E+00 2Q50 2R7.14286E-02 2348R0.00000E+00   T
/
/------------- BLOCK VI (BOUNDARY CONDITIONS) ---------
/
/ var   type  Group albedos
ibback=1   47R1
ibfrnt=0
jbeast=1   47R1
jbwest=0
kbsout=1   47R1
kbnort=1   47R1        T
/
/------------- BLOCK VII (PRINTING CONDITIONS) ---------
/
/
nxspr=0 nmatpr=1 ngeopr=1 nsrcpr=0 nsumpr=1
meshpr=2I-1 -4
nfdump=1 nsdump=0 njdump=0
nadump=0     T
```

APPENDIX E
DETECTOR RESPONSE SCRIPT

```
function [r1,r2,r3,r4,r5,r6,r7,r8]=
detResponse(bfiss,bimp,bsrc,Imp,Impg,bmult,fBU,fcoolTime,fRexp,fmult)
%function
[r1,r2,r3,r4,r5]=detResponse(bfiss,bimp,bsrc,Imp,impg,burnmult,fBU,fcoolTime,
fRexp);
%input:
%bfiss      account for subcritical multiplication? (testing purposes)
%bimp account for detector FOV? (testing purposes)
%bsrc account for source non-linearity w/ burnup (testing purposes)
%imp  neutron importance (from readImportance)
%impg gamma importance (from readImportance)
%bmult      burnup multiplier (to account for errors in predicted local
burnup)
%
%output:
%r1   predicted neutron response
%r2   predicted neutron response uncertainty due to 1% burnup uncertainty
%r3   experimental response vs. predicted
%r4   experimental response in x,y form
%r5   sum of squares error
%r6   gamma to neutron ratio
%r7   normalized gamma to neutron ratio
%r8   predicted gamma uncertainty

fuelType=1; %only NU fuel

%read in assembly configuration
BU=textread(fBU)';
coolTime=textread(fcoolTime)';
Rexp=textread(fRexp);
nx=size(BU,1);
ny=size(BU,2);

%read in source database
[sdat,budat,tdat]=srcrd2('nu2.src');
[sdatg,budatg,tdatg]=srcrd2('nu2g.src');

%Interpolate source distributions
tBU=reshape(BU,[nx*ny,1])*bmult;
tt=reshape(coolTime,[nx*ny,1]);
Sint=sourceInterp2(sdat,budat,tdat,tBU,tt);
Sint01=sourceInterp2(sdat,budat,tdat,tBU*1.01,tt);
Sg=sourceInterp2(sdatg,budatg,tdatg,tBU,tt);
Sg01=sourceInterp2(sdatg,budatg,tdatg,tBU*1.01,tt);
nG=size(Sint,3);
nGg=size(Sg,3);
Sint=reshape(Sint,[nx,ny,3,nG]);
Sint01=reshape(Sint01,[nx,ny,3,nG]);
Sg=reshape(Sg,[nx,ny,3,nGg]);
Sg01=reshape(Sg01,[nx,ny,3,nGg]);

%calculate sub-critical multiplication
SintTot=sum(sum(Sint,4),3);
```

```
Smult=fissionMatrix(fuelType,nx,ny,SintTot,BU,coolTime);
Sfiss=calcFiss(Smult,Sint);
Sfiss01=calcFiss(Smult,Sint01);

Stot=Sint+Sfiss;
Stot01=Sint01+Sfiss01;

%calibrate the efficiency to the measured data
Eff=calibrate(Rexp,Imp,Stot,Stot01);

%predict detector responses
[Rcalc,rerr]=calculateR(Eff,Imp,Stot,Stot01);
[Rcalcg,rgerr]=calculateR(1,Impg,Sg,Sg01);

%calculate sum of squares error of predicted vs. measured
rnew=zeros(nx+1,ny+1);
sumsq=0;
for i=1:size(Rexp,1)
    rnew(Rexp(i,1),Rexp(i,2))=Rexp(i,3);
    sumsq=sumsq+(Rexp(i,3)-Rcalc(Rexp(i,1),Rexp(i,2)))^2;
    Rexp(i,4)=Rcalc(Rexp(i,1),Rexp(i,2));
end

r1=Rcalc;
r2=rerr;
r3=Rexp;
r4=rnew;
r5=sumsq;
r6=Rcalcg./r1;
r7=r6/mean(mean(r6));
r8=rgerr./Rcalcg;
end

function y=calcFiss(Smult,Sint)
s=Sint;
for ix=1:size(Smult,1)
    for iy=1:size(Smult,2)
        SintTot=sum(sum(Sint(ix,iy,:,:)));
        s(ix,iy,:,:)=Sint(ix,iy,:,:)*(Smult(ix,iy))/(SintTot+1e-10);
    end
end
y=s;
end

function y=calibrate(r,imp,s,s01)
x=zeros(size(r,1),1);
for iexp=1:size(r,1)
    [x(iexp),err]=getR(1,r(iexp,1),r(iexp,2),imp,s,s01);
end
tr=r(:,3);
eff=sum(x.*tr)/sum(x.*x);
y=eff;
end

%calculate response for each detector location
function [y,yerr]=calculateR(eff,imp,s,s01)
nx=size(s,1); ny=size(s,2);
```

```
r=zeros(nx+1,ny+1); err=zeros(nx+1,ny+1);
for ix=1:(nx+1)
    for iy=1:(ny+1)
        [r(ix,iy),err(ix,iy)]=getR(eff,ix,iy,imp,s,s01);
    end
end
y=r;
yerr=err;
end

%calculate response and error for a single detector location
function [y,err]=getR(eff,ix,iy,imp,s,s01)
nx=size(s,1); ny=size(s,2);

%distance from detector to each assembly
indx=(ix-2:ix+1);
indx=indx(indx>0);indx=indx(indx<(nx+1));
indy=(iy-2:iy+1);
indy=indy(indy>0);indy=indy(indy<(ny+1));
iix=indx-ix+1;
iix=abs(iix-(iix<1));
iiy=indy-iy+1;
iiy=abs(iiy-(iiy<1));

%calculate R=IMP*S
rt=imp(iix,iiy,1:3,:).*s(indx,indy,1:3,:);
rt01=imp(iix,iiy,1:3,:).*s01(indx,indy,1:3,:);
rtt=sum(sum(rt,4),3);
rtt01=sum(sum(rt01,4),3);
dr=rtt01-rtt;
err=eff*sqrt(sum(sum(dr.^2)));
r=eff*sum(sum(sum(sum(rt))));
y=r;
end
```

LIST OF REFERENCES

1. Y. HAM, G. BOSLER, J. VONES, E. GRYNTAKIS, R. ABEDIN-ZADEH and O. PEIXOTO, “Neutron Measurement Techniques for Verification of Closely Packed Spent Fuel Assemblies Stored in a Spent Fuel Pond,” *Proc. of the INMM 48th Annual Meeting,* Tucson, AZ*,* July 8-12, 2007, Institute of Nuclear Materials Management (2007).

2. E. E. LEWIS and W.F. MILLER, *Computational Methods of Neutron Transport,* American Nuclear Society, La Grange Park, Illinois (1993).

3. W. WALTERS, A. HAGHIGHAT, M. WENNER, Y. HAM and S. SITARAMAN, “Methodology and Determination of Field of View of Neutron and Gamma Detectors in the Atucha Spent Fuel Storage Pool,” *Proc. of the INMM 50th Annual Meeting*, Tucson, AZ, July 12-16, 2009, Institute of Nuclear Materials Management (2009).

4. W. WALTERS, A. HAGHIGHAT, M. WENNER, Y. HAM and S. SITARAMAN, “Calculation of Sub-critical Multiplication Using a Simplified Fission Matrix Method,” *Proc. of the American Nuclear Society Winter Meeting*, Washington, DC, Nov. 15-19, 2009, American Nuclear Society (2009).

5. G. E. SJODEN and A. HAGHIGHAT, *PENTRAN-Parallel Environment Neutral Particle TRANsport Version 9.4x.5*, Code Manual/Users Guide, University of Florida, Nuclear & Radiological Engineering Department (November 2008).

6. X-5 MONTE CARLO TEAM, “MCNP – A General Monte Carlo N-Particle Transport Code, Version 5,” Vol. I, LA-UR-03-1987, Los Alamos National Laboratory (2003).

7. I.C. GAULD, S.M. BOWMAN, and J.E. HORWEDEL, *ORIGEN-ARP: Automatic Rapid Processing for Spent Fuel Depletion, Decay and Source Term Analysis, SCALE5.1 Manual*. Oak Ridge National Laboratory, Oak Ridge, TN (2006).

8. *SCALE: A Modular Code System for Performing Standardized Computer Analyses for Licensing Evaluations*, ORNL/TM-2005/39, Version 5.1, Vols. I-III; available as CCC-732 from Radiation Safety Information Computational Center, Oak Ridge National Laboratory (November 2006).

9. “Heavy water reactors: status and projected development,” International Atomic Energy Agency Technical Reports Series No. 407, IAEA, Vienna (2002).

10. L. A. ALVAREZ, J. CASARIO, J. FINK, R. PEREZ, M. HIGA, “Extended Burnup with SEU Fuel in Atucha–1 NPP,” *Proceedings of IAEA Technical Committee Meeting*, San Carlos de Bariloche, Argentina (November 1999).

11. E.W. LEMMON, M.O. MCLINDEN and D.G. FRIEND, "Thermophysical Properties of Fluid Systems" in NIST Chemistry WebBook, NIST Standard Reference Database Number 69, Eds. P.J. Linstrom and W.G. Mallard, National Institute of Standards

and Technology, Gaithersburg MD, http://webbook.nist.gov, (retrieved October 29, 2009).

12. C. YI, *PENMSH Express Manual*, Users Guide, University of Florida, Nuclear and Radiological Engineering Department (2007).

13. "BUGLE-96: Coupled 47 Neutron, 20 Gamma-Ray Group Cross Section Library Derived from ENDF0B-VI for LWR Shielding and Pressure Vessel Dosimetry Applications," DLC-76, Oak Ridge National Laboratory (Mar. 1996).

14. T. MOCK, K. MANALO, T. PLOWER and G. SJODEN, *DEV-XS: A Cross Section Development Primer for PENTRAN/PENBURN Version 2.0*, University of Florida, Nuclear and Radiological Engineering Department (2007).

BIOGRAPHICAL SKETCH

William Jonathan Walters was born and grew up in Vancouver, British Columbia, Canada in 1983. He attended the University of British Columbia and received a Bachelor of Applied Science degree in Engineering Physics in 2007. Upon graduation, he enrolled for graduate studies at the University of Florida under Dr. Alireza Haghighat. William received an MSc in Nuclear Engineering Sciences in 2009 and plans to continue studies in the PhD program.